MULTI-CENTENNIAL RESPONSE OF ENSO UNDER VARYING ATMOSPHERIC CO2

by

Jay R. Alder

A RESEARCH PAPER

submitted to

THE GEOSCIENCES DEPARTMENT

in partial fulfillment of the
requirements for the
degree of

MASTER OF SCIENCE

GEOGRAPHY PROGRAM

November 2009

Directed by
Dr. S. W. Hostetler

Acknowledgements

I thank my advisor Steve Hostetler for his outstanding and unwavering support and encouragement, Alan Mix, Nick Pisias and Jeff Shaman for their instruction and guidance. I am grateful to David Pollard for his assistance with implementing and modifying GENMOM, and for producing such a great model. Finally, I thank my wife Debbra for her editing and patience.

Table of Contents

Table of Figures

List of Tables

MULTI-CENTENNIAL RESPONSE OF ENSO UNDER VARYING ATMOSPHERIC CO2

The El Niño/Southern Oscillation (ENSO) affects millions of people via global teleconnections in the form of drought and torrential rainfall that impact agriculture and food production in many countries. Yet how ENSO will respond to a warming world is uncertain and a greatly debated topic. The Intergovernmental Panel on Climate Change Fourth Assessment Report (IPCC AR4) reports on modeling efforts using coupled atmospheric and oceanic general circulation models (AOGCMs) to diagnose the response of ENSO in a warming world. The IPCC stresses the value of a multi-model approach so that no one model is relied on too heavily and collections of models can be aggregated in ensembles to evaluate the quality of the current state of climate models. A formal evaluation of model ensembles used in the IPCC reports also fulfills a secondary goal of determining whether climate models are collectively improving over time. Here we present a new AOGCM, GENMOM, which combines the GENESIS atmospheric GCM (Global ENvironmental and Ecological Simulation of Interactive Systems) and MOM (Modular Ocean Model). GENMOM simulates a realistic present-day climate and ENSO dynamics that are on par with the models used in IPCC AR4. The response of ENSO to doubling atmospheric CO_2 from 355 ppmV to 710 ppmV and 1420 ppmV (hereafter denoted 1x, 2x and 4x respectively) is evaluated using long (600 year) GENMOM simulations. Higher amplitude and more frequent ENSO events are associated with global warming.

1. Introduction

ENSO is a coupled ocean-atmosphere mode of variability that occurs in the Pacific Ocean (Neelin et al., 1998). The phase of ENSO is identified by warm (El Niño) or cold (La Niña) sea surface temperature (SST) anomalies along the equator and the sea level pressure difference between Tahiti and Darwin, Australia (Horel and Wallace, 1981). An El Niño event is a disruption of the Walker Circulation, which is the east-west atmospheric circulation system along the Tropical Pacific that strongly influences the location of Pacific rainfall. The disruption occurs when the easterly trade winds relax which reduces cold ocean upwelling along the coast of South America which in turn results in a weakening of the normal east-west temperature gradient in the tropical Pacific. Warm western surface waters and rainfall propagate eastward. The La Niña event is the opposite of El Niño, whereby the easterly trade winds strengthens, which enhances upwelling along the coast of South America resulting in a stronger east-west surface temperature gradient (Neelin et al., 1998).

Neither the ocean nor the atmosphere trigger an ENSO event in isolation, they are inherently linked (Trenberth, 1997; Neelin et al., 1998). Historical observations indicate the frequency of ENSO is between 3 - 7 years. Warm and cold ENSO events can have global teleconnections that are expressed as anomalies of temperature and precipitation. Significant progress has been made over the past two decades in understanding the mechanism of ENSO and related hydrological teleconnections (Giannini et al. 2001, Ropelewski and Halpert, 1987). The long-term behavior of ENSO outside the historical record and under radiative forcing associated with varying atmospheric composition and large-scale boundary conditions (e.g., continental ice sheets) that occurred in the past

(Clement et al., 1999), and that might occur in the future (Collins, 2000a, Collins, 2000b), is of interest for extending our understanding of ENSO to interpret past and future climatic change and variability. Modeling past and future ENSO characteristics is best accomplished through the application of coupled atmospheric and oceanic general circulation models and many related model studies have been published (eg, Otto-Bliesner et al. 2003; Liu and Wu, 2000; Timmermann et al., 1999; Merryfield, 2006).

Here we present a new AOGCM, GENMON, that combines GENESIS (Global ENvironmental and Ecological Simulation of Interactive Systems) and MOM (Modular Ocean Model) general circulation models. Both models have been used widely in climate studies that demonstrate their overall ability to produce climate simulations that are in agreement both with observations and with similar models. Our current version of GENMOM uses T31 (~3.75° x 3.75° latitude and longitude) horizontal resolution for both the atmosphere and ocean to balance computational requirements with the ability to simulate features of the general circulation. The model is also used to derive time-varying 6-hour histories of atmospheric SST fields that are used to drive our high-resolution regional climate model over regions of interest (eg, Hostetler and Giorgi, 1995; Hostetler et al., 2000).

We apply GENMOM to explore the multi-century ENSO response to present, doubled and quadrupled atmospheric CO_2 levels (1x, 2x and 4x, respectively). We first compare the simulation of present-day climatology with observations and with other AOGCMs used in the IPCC AR4. We then compare the GENMOM ENSO response with other IPCC models and present a detailed analysis of the characteristics of long-term ENSO response of GENMOM to atmospheric CO_2 forcing.

2. GENMOM description

a. GENESIS description

GENESIS has been developed with emphasis on terrestrial physical and biophysical processes, and suitability for paleoclimatic experiments. Earlier versions of GENESIS are described by Thompson and Pollard (1995; 1997) and Pollard and Thompson (1994, 1995, 1997), and have been applied and tested in a wide range of modern and paleoclimate applications (e.g., Bice et al., 2006; Beckmann et al., 2005; DeConto et al., 2006, 2008; Horton et al., 2007; Hostetler et al., 2006; Joussaume et al., 1999 Miller et al., 2005; Pinot et al, 1999; Poulsen et al., 2006, 2007; Ruddiman et al., 2005).

The nominal AGCM resolution is spectral T31 (3.75° x 3.75°) with 18 vertical levels. Spectral transform dynamics are used for mass, heat and momentum (Williamson et al., 1987). A semi-Lagrangian transport in grid space is used for water vapor (Williamson and Rasch, 1989). Convection in the free atmosphere and in the planetary boundary layer is treated using an explicit sub-grid buoyant plume model similar to, but simpler than, Kreitzberg and Perkey (1976) and Anthes (1977, section 4). Stratus, convective and anvil cirrus clouds are predicted using prognostic 3-D water cloud amounts, (Smith, 1990; Senior and Mitchell, 1993) and clouds are advected by semi-Lagrangian transport and mixed vertically by convective plumes and background diffusion.

A land-surface transfer model (Land Surface eXchange) accounts for the physical effects of vegetation (Pollard and Thompson, 1995). Up to two vegetation layers (trees and grass) can be specified at each grid point, and the radiative and turbulent fluxes

through these layers to the soil or snow surface are calculated. A six-layer soil model extends from the surface to 4.25 m depth, with layer thicknesses increasing from 5 cm at the top to 2.5 m at the bottom. Physical processes in the vertical soil column include heat diffusion, liquid water transport (Clapp and Hornberger, 1978; Dickinson, 1984), surface runoff and bottom drainage, uptake of liquid water by plant roots for transpiration, and the freezing and thawing of soil ice. A three-layer snow model, which includes fractional area cover when the snow is thin, is used for snow cover on soil, ice-sheet and sea-ice surfaces. A three-layer sea-ice model accounts for local melting, freezing, fractional ice cover (Semtner, 1976; Harvey, 1988), and includes sea-ice dynamics associated with wind and ocean current using the cavitating-fluid model of Flato and Hibler (1992). Version 3 of GENESIS (Zhou et al., 2008; Kump and Pollard, 2008) incorporates the NCAR CCM3 radiation code (Kiehl et al., 1998) and the ocean is represented by the MOM2 ocean general circulation model (Pacanowski, 1996).

b. MOM2 description

MOM2 was developed by the Geophysical Fluid Dynamics Laboratory (GFDL) circa the early 1990s, but builds off previous work that stretches back to 1969 (Pacanowski, 1996). MOM2 is a finite difference implementation of the primitive equations of ocean circulation using the Navier-Stokes equations with the Boussinesq, hydrostatic, and rigid lid approximations (Bryan, 1969). The Boussinesq approximation assumes constant density with depth as opposed to density varying as a function of depth, which greatly reduces computational complexity. The hydrostatic approximation assumes that vertical pressure gradients are due only to density. A nonlinear equation of state couples temperature and salinity to fluid velocity. An insulating boundary is used

such that no temperature or salinity flux is exchanged between ocean and land cells. Unlike the sigma levels used for atmospheric altitude in GENESIS, MOM uses a fixed z-axis for depth, which simplifies the equations used in the finite difference techniques. The version of MOM2 used here also has the ability to use oxygen isotopes as a tracer, which was not used in this study.

c. GENMOM coupling

To simplify the coupling between the atmosphere and ocean, both the GCMs are implemented on essentially the same T31 grid. In the OGCM, the latitudinal grid spacing is not exactly T31, but is adjusted with a cosine-stretching factor (Pacanowski, 1996) to closely approximate T31. GENESIS and MOM2 interact in an essentially synchronous manner: 6-hr averages of the fluxes of heat, water, and momentum are passed to the OGCM from the AGCM and the resulting updated SSTs are averaged over 6 hours and passed back to the AGCM. Sea-ice is treated by the AGCM (LSX) and sea-ice related fluxes are passed to the OGCM between the sea-ice base and the uppermost ocean layer. Continental freshwater river runoff is globally averaged and spread over the world ocean.

3. Simulation of the present climate

In this section we analyze the annual and seasonal climatology for a 30-year period (model years 970 – 999), which are sampled from the last 600 years of the present-day simulation. We select this period because it is the last 30 years of the simulation and is fully equilibrated. Where possible, we compare the GENMOM results to ensembles of the AOGCMS used in the IPCC AR4 (Randall et al., 2007). Similarly, we use the last 30 years of the Climate of the 20th Century experiment from eight select IPCC AR4 models (Table 1) to provide context for evaluating the performance of

GENMOM. For the present-day GENMOM simulation, atmospheric CO_2 concentration is prescribed at 355 ppmV. The model was initialized with a latitudinal dependent temperature profile while salinity is uniformly prescribed at 35 ppt. We then integrated GENMOM continuously for 1000 years. Analysis of ocean temperatures indicates that spin up of the model was essentially achieved after 400 years.

a. Validation datasets and input files

In contrast to the IPCC AR4 wherein a variety of observed datasets are used to evaluate model performance, whenever possible we rely solely on the NOAA NCEP Reanalysis 2 data set (NCEP2, Kanamitsu, et al., 2002) to maintain consistency among variable fields. NCEP2 is a data assimilation and synthesis product that incorporates a massive array of in situ and satellite based observations. The observed data are synthesized together in the reanalysis global model (Kalnay et al., 1996), which provides a large, consistent, and interrelated set of atmospheric fields such as temperature, pressure, and wind velocity. In addition to synthesizing observed datasets, the NCEP model provides simulated estimates for fields that are not well observed, such as soil moisture. Because the reanalysis relies on a climate model, NCEP is not a perfect representation of the real world and numerous studies have quantified uncertainties in NCEP data (Trenberth and Guillemot, 1998, Trenberth et al., 2001, Smith et al., 2004). We use a standard climatology period of 1981-2005 for the NCEP data unless otherwise specified.

Observed SST data are from the NOAA Optimum Interpolation Sea Surface Temperature V2 (OI SST, Reynolds, et al., 2002), which is a 1° x 1° gridded dataset derived from in situ and satellite data. We use a climatology period of 1982-2005 for OI

SST, where 1982 is the first full year the data are available. Global subsurface ocean temperatures are obtained from The World Ocean Atlas 2005 (WOA05, Locarnini et al., 2006), which is 1° x 1° gridded dataset for ocean temperature at specific depths. The data are acquired by bottle samples, Mechanical Bathythermograph (MBT), ship-deployed Conductivity-Temperature-Depth (CTD) package, Digital Bathythermograph (DBT), Expendable Bathythermograph (XBT), profiling float, moored and drifting buoys, gliders, and undulating oceanographic recorder (UOR).

GENMOM input files for topography, bathymetry and the land-ocean distribution mask are derived by interpolating the ICE-4G model (Peltier, 2002) reconstruction from 1° x 1° to T31 resolution. To maintain numerical stability in MOM2 we smooth the bathymetry field derived from ICE-4G with a 9-cell moving window average. Modern values for the distribution of vegetation, soil texture and freshwater lakes are prescribed. The use of ICE-4G to derive global topography and bathymetry is based on our goal of simplifying configuration of GENMOM for paleoclimate applications.

Table 1: Eight AOGCMs used in the IPCC AR4. T indicates the horizontal resolution using spectral truncation. L indicates the number of levels used in the model.

Model	Modeling Center, Country	Atmosphere Resolution	Ocean Resolution
CCCMA CGCM 3.1 T63	Canadian Centre for Climate Modelling and Analysis, Canada	T47 (~2.8° x 2.8°) L31 McFarlane et al., 1992; Flato, 2005	1.9° x 1.9° L29 Pacanowski et al., 1993
CSIRO MK 3.0	Commonwealth Scientific and Industrial Research Organisation (CSIRO) Atmospheric Research, Australia	T63 (~1.9° x 1.9°) L18 Gordon et al., 2002	0.8° x 1.9° L31 Gordon et al., 2002
GFDL CM 2.0	U.S. Department of Commerce/National Oceanic and Atmospheric Administration (NOAA)/Geophysical Fluid Dynamics Laboratory (GFDL), USA	2.0° x 2.5° L24 GFDL GAMDT, 2004	0.3°–1.0° x 1.0° Gnanadesikan et al., 2004
MIROC 3.2 medres	Center for Climate System Research (University of Tokyo), National Institute for Environmental Studies, and Frontier Research Center for Global Change (JAMSTEC), Japan	T42 (~2.8° x 2.8°) L20 K-1 Developers, 2004	0.5°–1.4° x 1.4° L43 K-1 Developers, 2004
MIUB ECHO-G	Meteorological Institute of the University of Bonn, Meteorological Research Institute of the Korea Meteorological Administration (KMA), and Model and Data Group, Germany/Korea	T30 (~3.9° x 3.9°) L19 Roeckner et al., 1996	0.5°–2.8° x 2.8° L20 Wolff et al., 1997
MPI ECHAM5	Max Planck Institute for Meteorology, Germany	T63 (~1.9° x 1.9°) L31 Roeckner et al., 2003	1.5° x 1.5° L40 Marsland et al., 2003
NCAR CCSM 3.0	National Center for Atmospheric Research, USA	T85 (1.4° x 1.4°) L26 Collins et al., 2004	0.3°–1° x 1° L40 Smith and Gent, 2002
UKMO HadCM3	Hadley Centre for Climate Prediction and Research/Met Office, UK	~1.3° x 1.9° L38 Pope et al., 2000	0.3°–1.0° x 1.0° L40 Gordon et al., 2000

b. Atmospheric fields

The gradient and distribution of the zonally averaged profile of air temperature simulated by GENMOM agrees well with the NCEP2 profile (Fig. 1). GENMOM simulates a cold bias above 30N in the Northern Hemisphere (NH) during both seasons. The Southern Hemisphere (SH) has a cold bias above 60S during austral summer. GENMOM simulates a noticeable cold bias in the uppermost atmosphere above the wintertime pole. Seasonally, GENMOM simulates the meridional shift of peak insolation and warmest surface temperatures well when compared to observations. However, the tropical warm region is slightly more meridionally narrow than observed and the shape is less convex.

In general, both pattern and magnitude of the annual planetary jet stream structure and easterly winds are well simulated in both DJF and JJA (Fig. 2). In both winter hemispheres the core of the jetstream (at ~200 hPa) and related upper level winds (500 hPa) are slightly enhanced relative to the NCEP2 data. These features are minor mismatches and suggest that GENMOM produces a realistic mean planetary-scale wind structure that is essential to related positions of the stormtracks.

Globally, GENMOM simulates the upper atmospheric flow and 500 hPa geopotential height well (Figure 3). During boreal winter the ridge over Western North America is shifted eastward in GENMOM and the associated trough to the east over Northern Canada and the North Atlantic is similarly slightly displaced relative to that of the NCEP data. The 500 hPa heights over North America and Eurasia are lower than those of the NCEP data resulting in slightly reduced wind velocities, particularly over eastern North America and the North Atlantic. In the SH, austral summer 500 hPa

heights are well simulated but wind velocities associated with the westerlies are somewhat reduced due to the lower pressure gradient over the southern ocean and Antarctica.

During boreal summer, the ridge over Western North America is correctly placed in GENMOM, but the amplitude of the ridge is greater than observed and the related downstream trough is slightly deeper than that of the NCEP data (Fig. 3). Heights in the region extending east of the Mediterranean and across India and China appear modestly lower than observed; however, part of the apparent discrepancy stems from values that are just above or just below the color breaks in the plotting scales. In the SH, the comparison for the austral winter is similar to that of the austral summer presented above.

Winter and summer sea level pressure (SLP) is well captured by GENMOM (Fig. 3). As is the case in the upper atmosphere, during boreal winter GENMOM simulates lower SLP in the Aleutian and Icelandic lows. As a result, wind velocities are enhanced over North America. In the SH, surface pressure and winds are comparable with those of the NCEP data except along Antarctica where SLP is higher and wind velocities are lower due to the reduced pressure gradient.

Boreal summer simulation of SLP and wind velocities are quite good; the subtropical highs in the NH are well placed and the associated wind velocities are comparable to NCEP. SLP and wind velocities in the tropics and the SH are also well simulated by GENMOM. The anomalously high pressure over the Southern Ocean does not corroborate with a warm SST bias. During austral summer, the SH high-pressure anticyclones are weaker than observed. The south Pacific high is poorly simulated and does not produce anticyclonic flow, which leads to a weakened South Pacific Gyre.

Westerly winds are simulated to be too weak in the Southern Ocean. GENMOM simulates stronger than observed westerly winds across southern Europe, which is caused by the overactive Icelandic low.

Atmospheric specific humidity simulated by GENMOM is in agreement with the NCEP data (Fig. 6). A slight dry bias is evident over the tropics and a wet bias is evident in the SH below 700 hPa which is associated with the warm bias in atmospheric temperature caused by a warm Southern Ocean. A wet bias over the NH below 700 hPa is not associated with a warm bias in atmospheric temperature; rather, it is caused by weaker-than-observed convection from the surface to ~400 hPa between 70N – 80N.

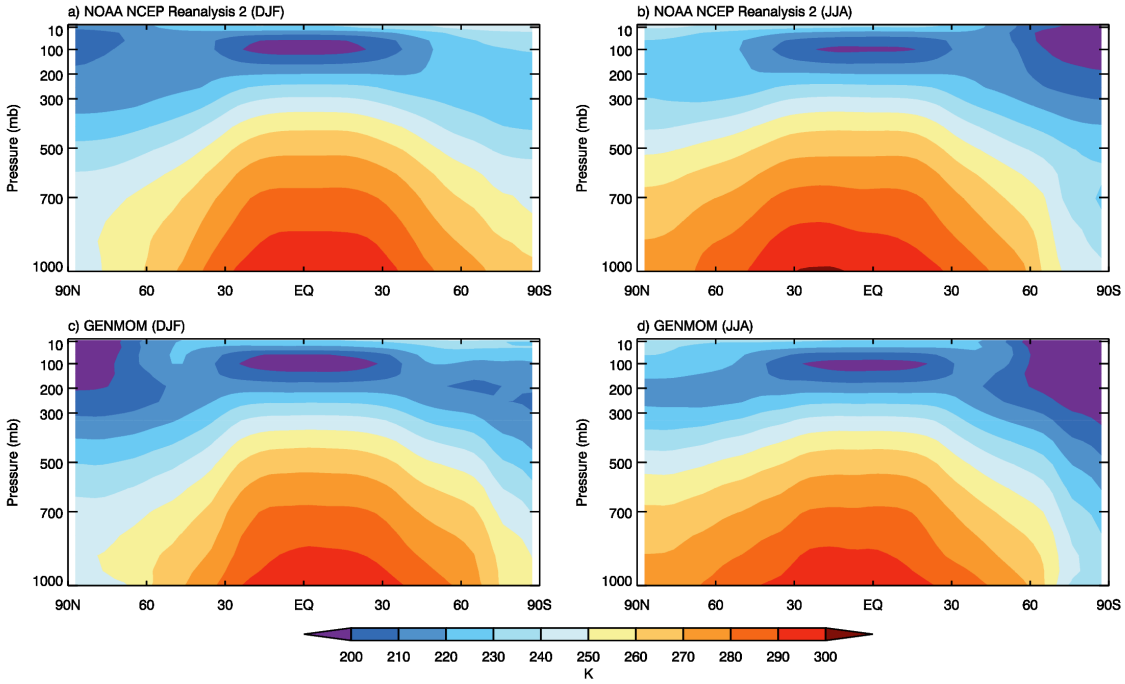

Figure 1: Mean-annual zonal averaged atmospheric temperature profiles. a) Observed DJF, b) Observed JJA, c) GENMOM DJF, d) GENMOM JJA.

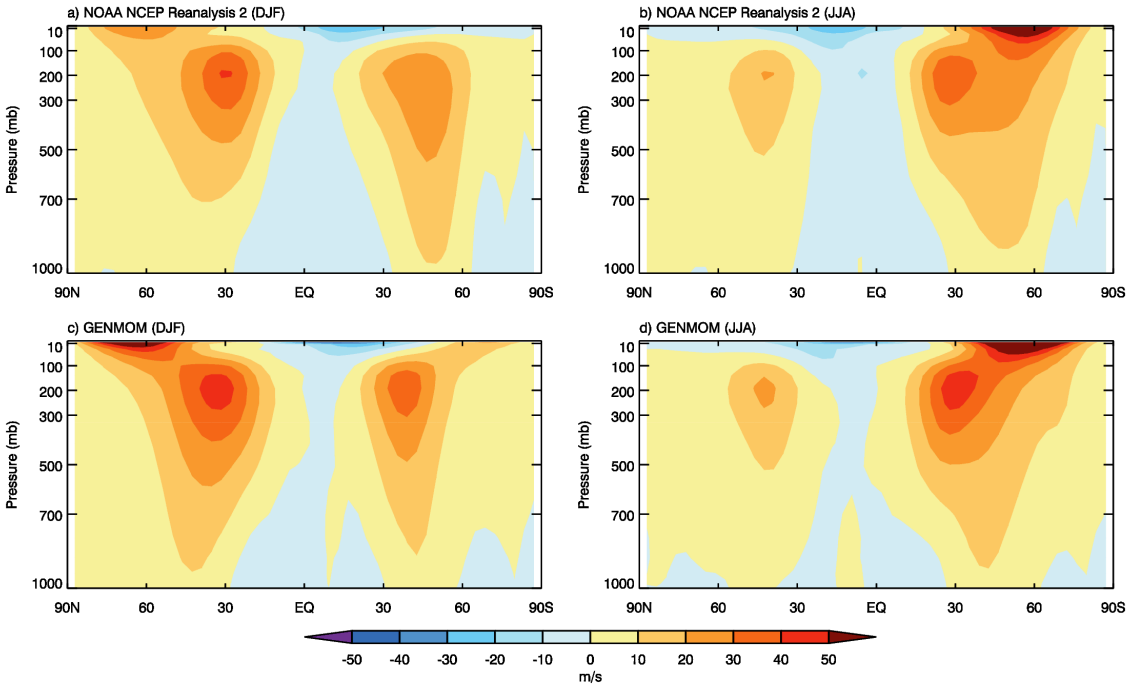

Figure 2: Winter (DJF) and summer (JJA) zonally averaged eastward wind velocity. a) Observed DJF, b) Observed JJA, c) GENMOM DJF, d) GENMOM JJA.

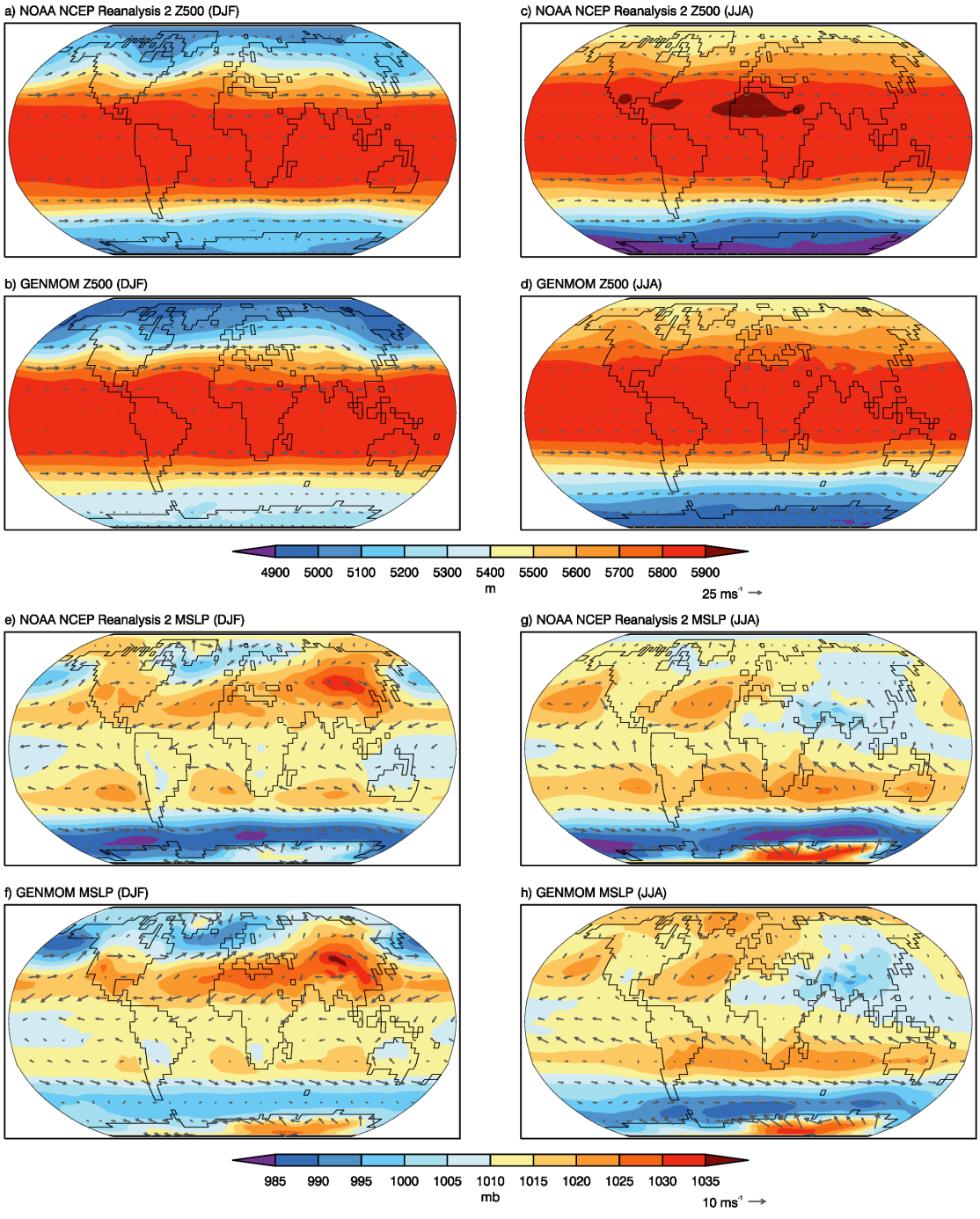

Figure 3: Mean sea level pressure (MSLP) and 500 hPa geopotential height (Z500) with wind vectors.

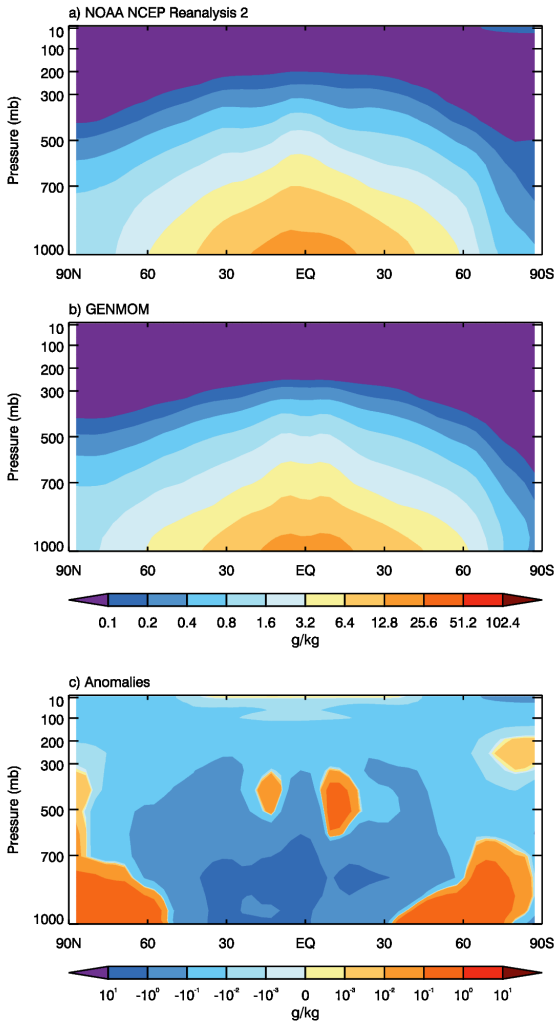

Figure 4: Mean-annual zonally averaged specific humidity profiles. a) Observed, b) GENMOM, c) Anomalies.

c. Modeled surface temperature

The simulated global mean-annual 2 m air temperature is 278.1 K, in good agreement with the NCEP2 value of 278.9 K. Over land the simulated temperature is 1.0 K colder than observations and over the oceans simulated temperature is 0.2 K warmer than observations. GENMOM simulates the meridional temperature gradient well. A warm bias is found over the Southern Ocean while a cold bias is simulated in the Norwegian Sea and Greenland (Fig. 5 and 6). In general, major topographic features resolved by the model such as the Rocky Mountains, the Andes and the Himalayas, have regional temperatures that match well to observation.

The Southern Ocean warm bias may be caused by an overactive modeled meridional heat transport that is stronger than actually exits, or weaker than observed westerly winds across the Southern Ocean (not shown), or both. The cold bias over the Norwegian Sea is caused by too much simulated sea-ice. Because the cold water tongue associated with the California Current is ~300 km wide, is not adequately resolved at T31, and leads to a warm bias along the Pacific coast of North America. The subgrid extent of the northward branch of the South Pacific Gyre also is not well resolved, resulting in weaker-than-observed cold water Humboldt Current along the western coast of South America. The weakened circulation results in a warm SST bias off the coast of Chile as well as westerly winds which are ~5 m sec^{-1} weaker than observations of ~7 m sec^{-1} (not shown).

We note that the high latitude temperature anomalies (Fig. 6) are partially attributed to a mismatch between the ICE-4G derived land mask and that of NOAA OI SST V2 interpolated to T31. Where a mismatch occurs, large anomalies are created due

to comparing a SST grid cell to a 2 m air temperature grid cell. In future applications of GENMOM, care should be taken to minimize such grid cell mismatches by ensuring that the model land-ocean distribution matches that of NOAA OI SST when the ICE-4G dataset is interpolated to T31.

The GENMOM simulation has many features in common with the IPCC models, including: 1) cold bias over northern Europe, 2) a warm SST bias in the waters west of South America, 3) a warm bias in the Southern Ocean and 4) cold biases over the Himalayas and Greenland (Fig. 6). In contrast to many of the IPCC AR4 models, GENMOM simulates the annual surface temperature over much of Antarctica with anomalies <2°C. Other IPCC A4 models such as CSIRO MK 3.0, MIUB ECHO-G and UKMO HadCM3 all simulate the majority of the Antarctic landmass with a 5+°C cold bias.

GENMOM overestimates the seasonal cycle in Greenland, South America, southeast United States and Australia while underestimating in Northern Africa, western United States and much of Europe and Asia (Fig. 7). The model also simulates greater variability over some of the oceans, particularly in the mid latitudes. GENMOM not only simulates a warm bias in the Southern Ocean, but also a more seasonally variable than observed Southern Ocean. Similar to Figure 6, grid cells where the land-ocean distribution does not match have large seasonal cycle amplitude anomalies.

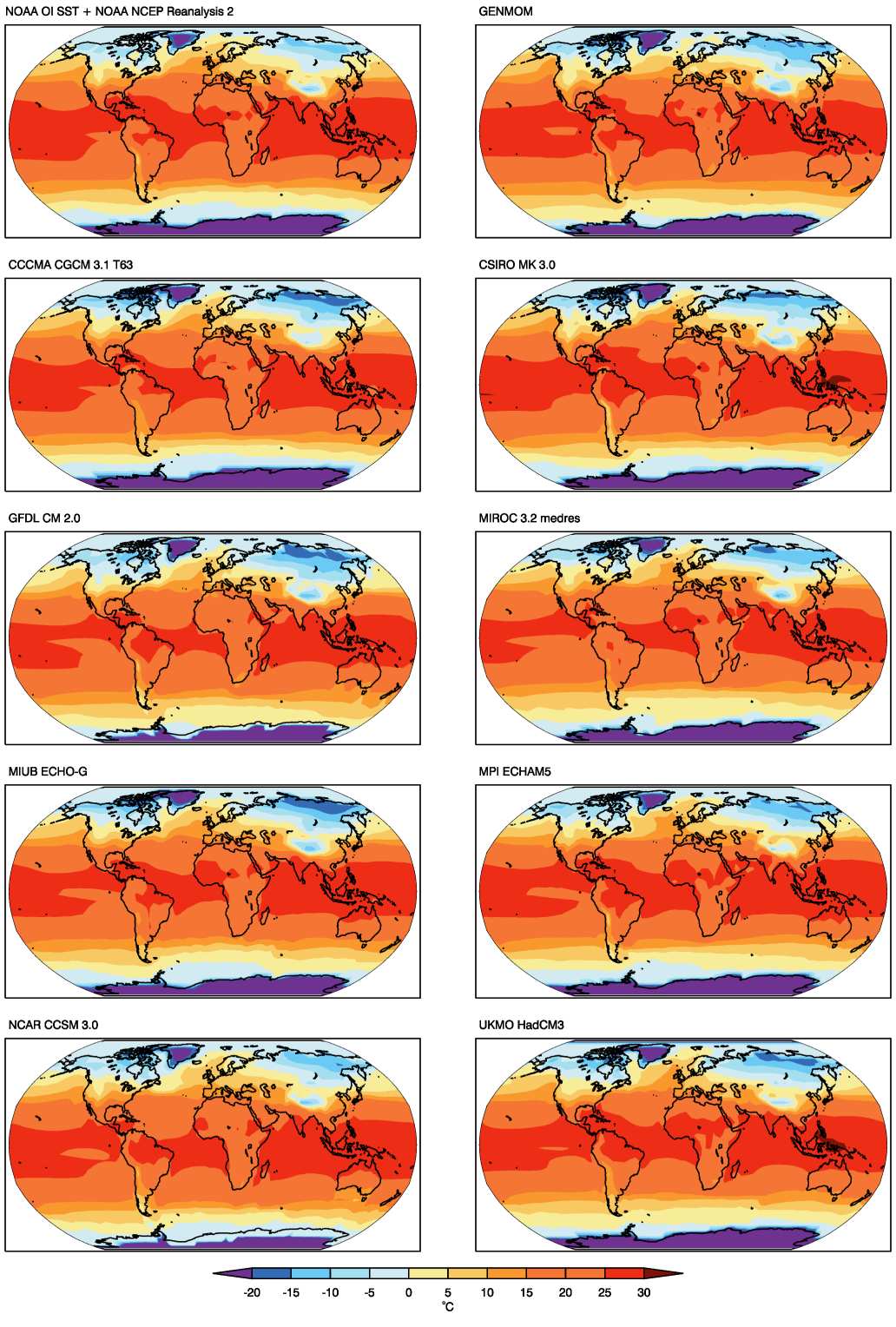

Figure 5: Observed and simulated surface temperature from GENMOM and 8 AOGCMs included in IPCC AR4. Observed data are from NOAA NCEP Reanalysis 2 (over land) and NOAA OI SST (over sea). GENMOM 2 m air temperature and SST are for model years 970-999 of the control equilibrium simulation. All IPCC AR4 models are averaged over the last 30 years of the Climate of the 20th Century experiment. All data are bi-linearly interpolated to a 5° x 5°grid.

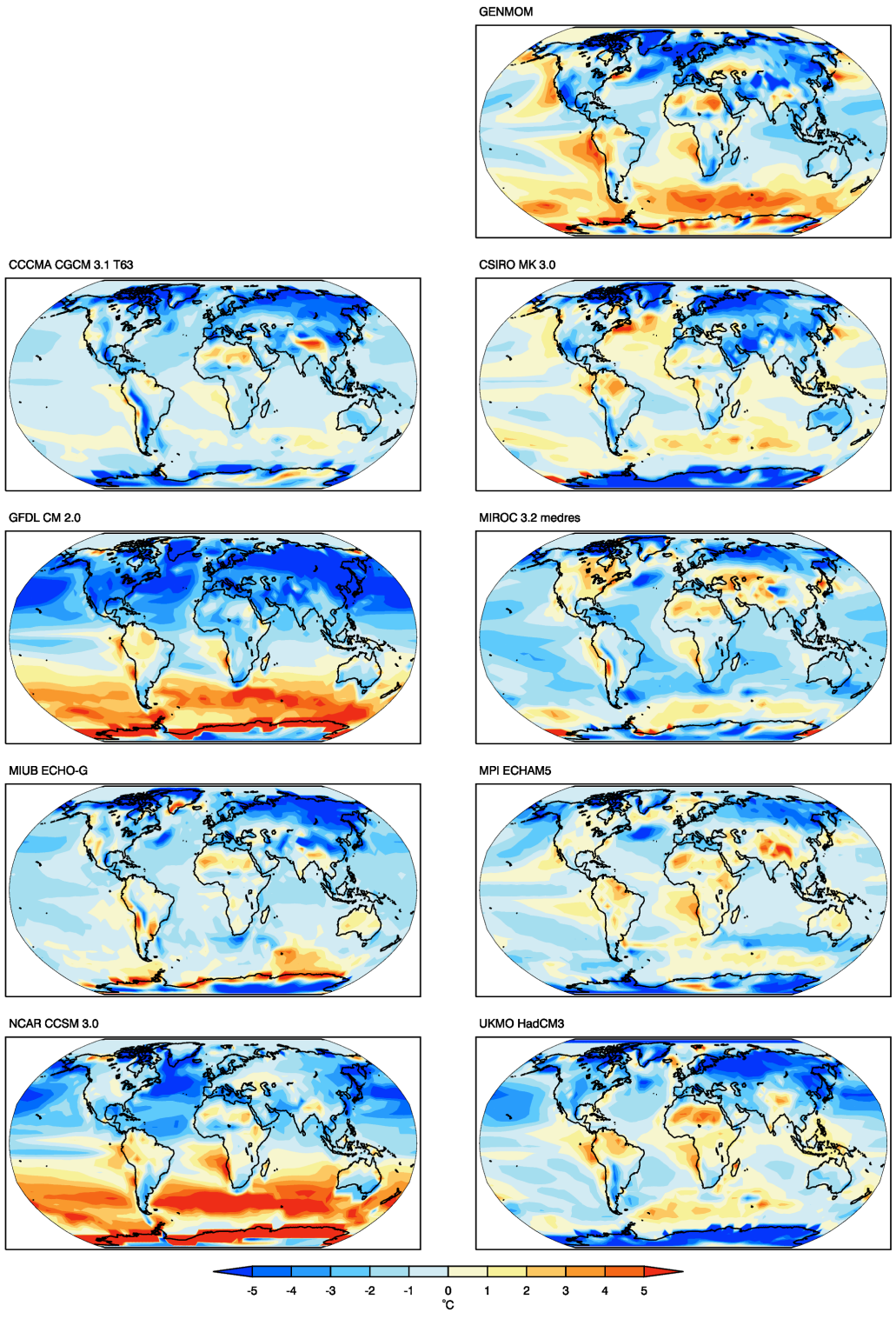

Figure 6: Anomalies between simulated and observed surface temperatures. Data are described in Fig 1.

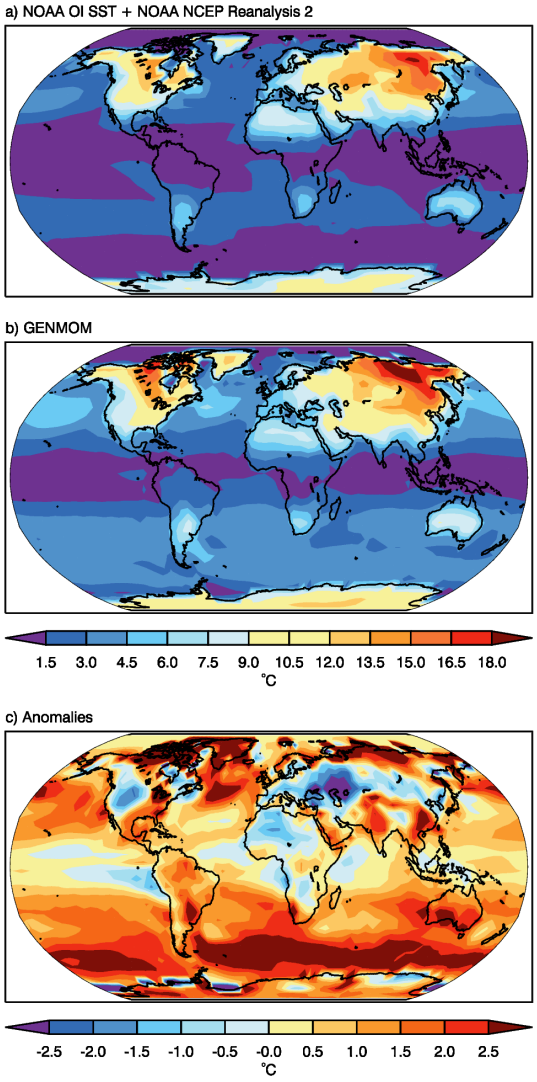

Figure 7: Observed and modeled seasonal cycle amplitude of 2 m air temperature and anomalies. The amplitude of the seasonal cycle calculated as the standard deviation of the 12 climatological months.

d. Precipitation

GENMOM simulates global mean-annual precipitation reasonably well relative to both observations and the IPCC models (Figs. 8, 9). Similar to other AOGCMs, GENMOM produces a split Intertropical Convergence Zone (ITCZ) in the tropical Pacific. The ITCZ is located where the NH trade winds converge with those of the SH resulting in upward motion in the atmosphere and deep convection, cloud formation and precipitation. The ITCZ migrates seasonally north and south in response to the seasonal cycle of maximum solar radiation in the tropics.

During DJF, the southern branch of the ITCZ simulated by GENMOM extends too far to the east. In JJA, the northern branch of the ITCZ simulated by GENMOM is compressed and extends too far to the north relative to observations. Lin (2007) found that many IPCC AR4 models produce a double ITCZ which is caused by: 1) excessive tropical precipitation, 2) very high sensitivity of modeled precipitation and surface air humidity to SST, 3) a lack of sensitivity of cloud amount to precipitation, and 4) a lack of sensitivity of stratus cloud formation to SST. GENMOM produces a cold SST bias in the Pacific Basin along with a confined cold tongue, both of which Lin (2007) noted as factors that result in a double ITCZ. Consistent with Lin (2007), GENMOM does not produce a significant double ITCZ when coupled to a slab ocean due to weakened ocean–atmosphere feedbacks. The double ITCZ problem can potentially be resolved by improving these ocean-atmosphere feedbacks. Globally, GENMOM underestimates seasonal DJF precipitation in the Indian Ocean and JJA precipitation over the southern Asian landmass as well as an underestimate of equatorial Atlantic precipitation.

The zonal annual mean profile of precipitation clearly illustrates the double ITCZ in GENMOM (Fig. 10); the double peak in total precipitation is evident at 10N and 10S rather than the observed single and stronger peak at 10N and 0N. Outside of the tropics however, the modeled precipitation compares well with observations and the selected IPCC AR4. The split in ITCZ precipitation notwithstanding, the overall precipitation field produced by GENMOM is a significant improvement over previous versions of GENESIS, which consistently over predicted precipitation due to simplified ocean heat transport forced with an observed ocean circulation.

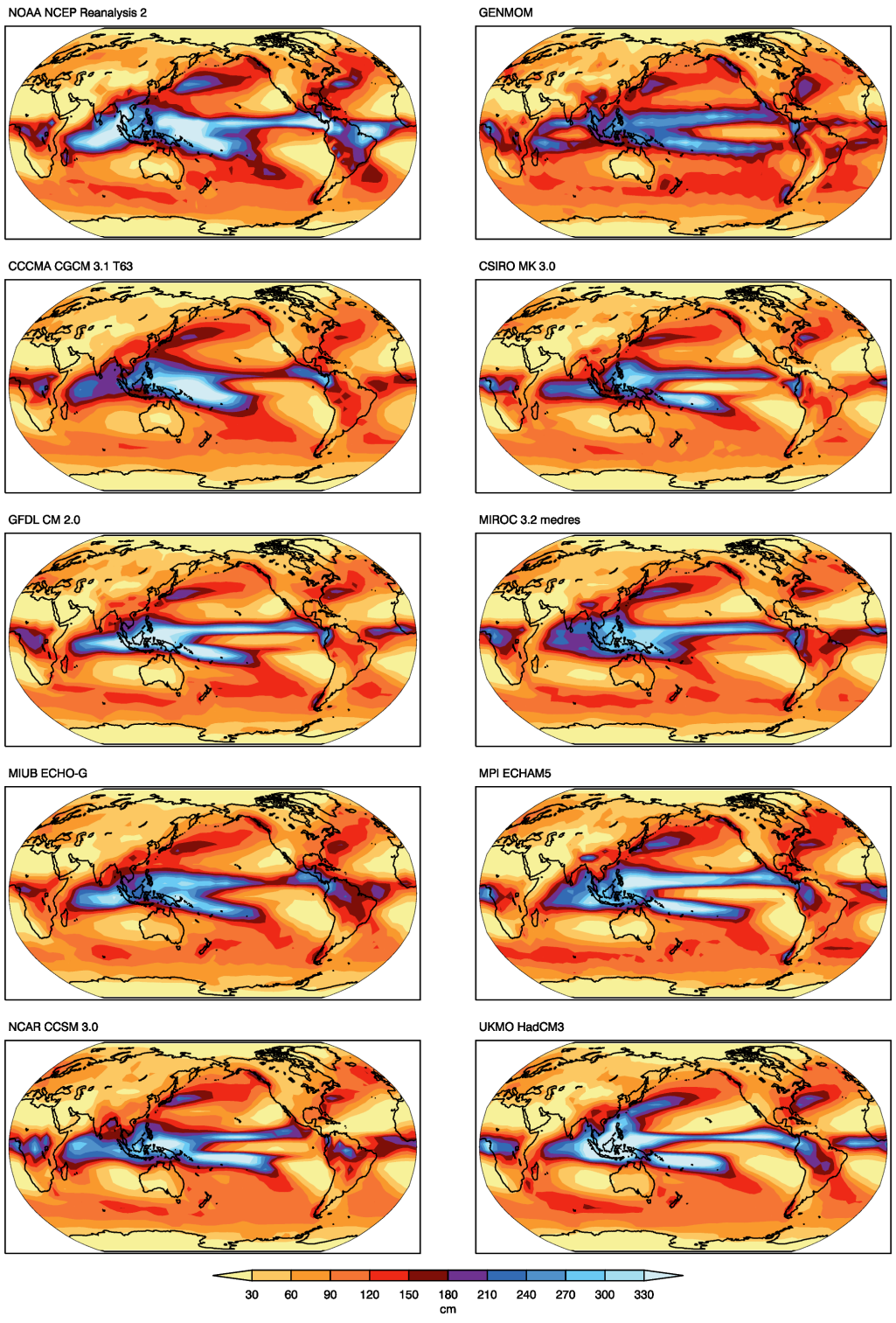

Figure 8: Observed and simulated annual total precipitation from GENMOM and 8 AOGCMs included in IPCC AR4. All data are bi-linearly interpolated to a 5° x 5°grid.

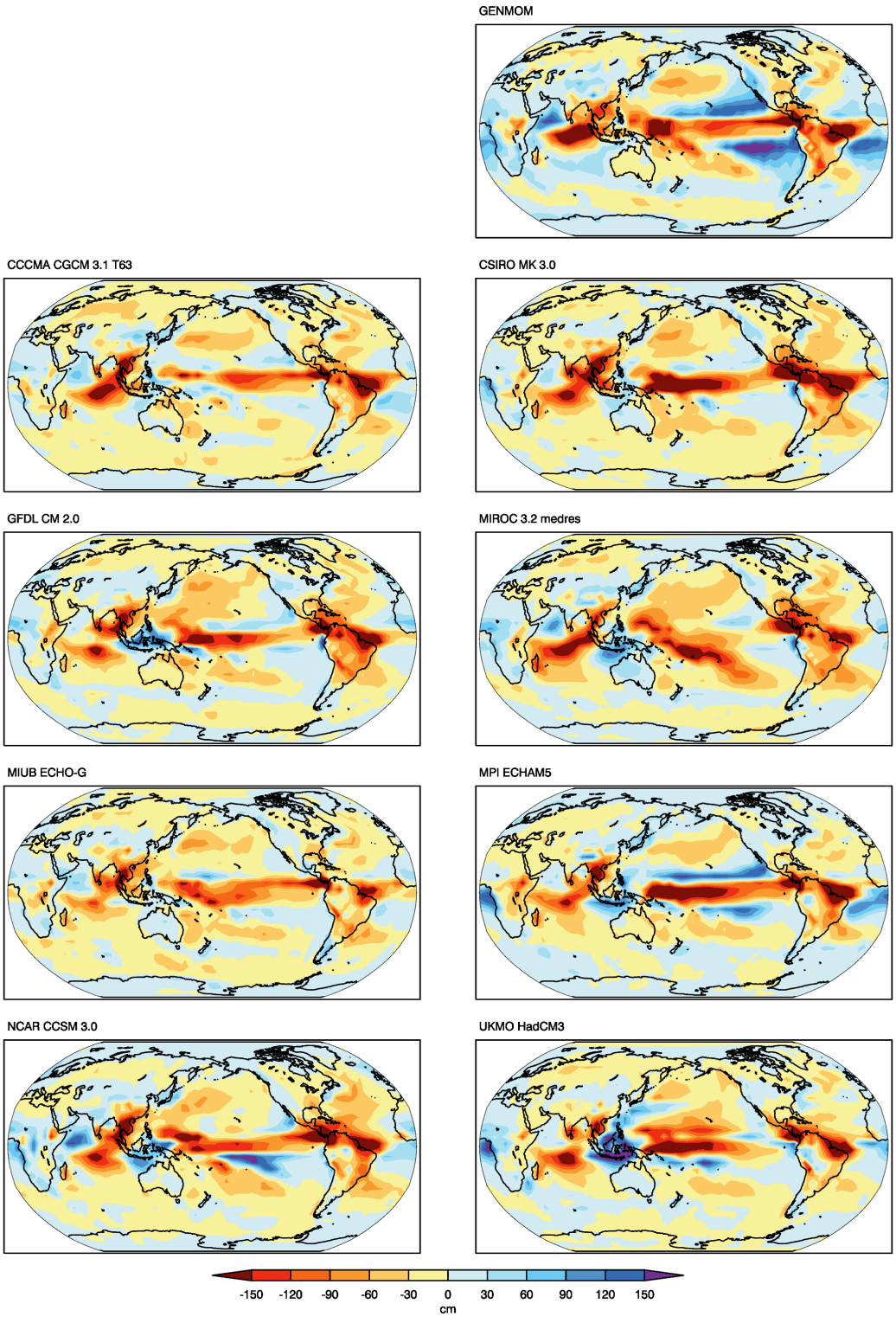

Figure 9: Anomalies between simulated annual total precipitation and observations.

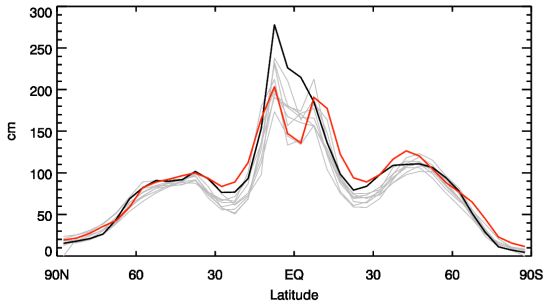

Figure 10: Annual zonal total precipitation for observations (black), GENMOM (red) and 8 IPCC AR4 models (gray).

e. Oceanic fields

In general, the surface and subsurface model ocean temperatures compare well to observations, the pattern and magnitude of the simulated temperature profile matches observations well. Exceptions include a cold bias at the surface and a warm bias in the mid-depths in the tropics (Fig. 11). A warm bias in the near-surface of the Southern Ocean is consistent with the surface temperature anomalies shown in Figure 6. The Southern Ocean warm bias may be caused by a large warm bias in the ocean mid-layers in the tropics. The warm bias in the tropical ocean mid-layers may be due to GENMOM failing to adequately simulate ocean circulation patterns that match observation or exhibiting a weaker-than-observed ocean heat transport.

GENMOM simulates winter sea-ice extent and concentration well in both hemispheres for both DJF and JJA (Fig. 12). Sea-ice extends too far into the Norwegian Sea during both winter and summer and too far into Hudson Bay during winter. Antarctica shows deficient sea-ice during summer, which is when the warm temperature bias in the Southern Ocean is at its strongest. Antarctic winter sea-ice extent matches that of the observations surprisingly well despite the Southern Ocean warm bias.

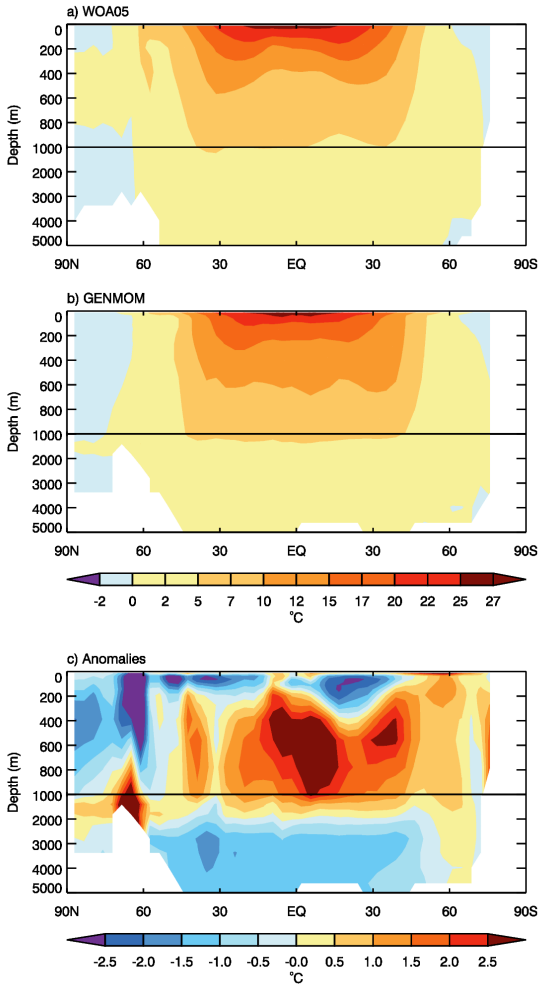

Figure 11: Mean-annual zonally averaged ocean temperature profile. a) Observed, b) GENMOM, c) GENMOM minus observed.

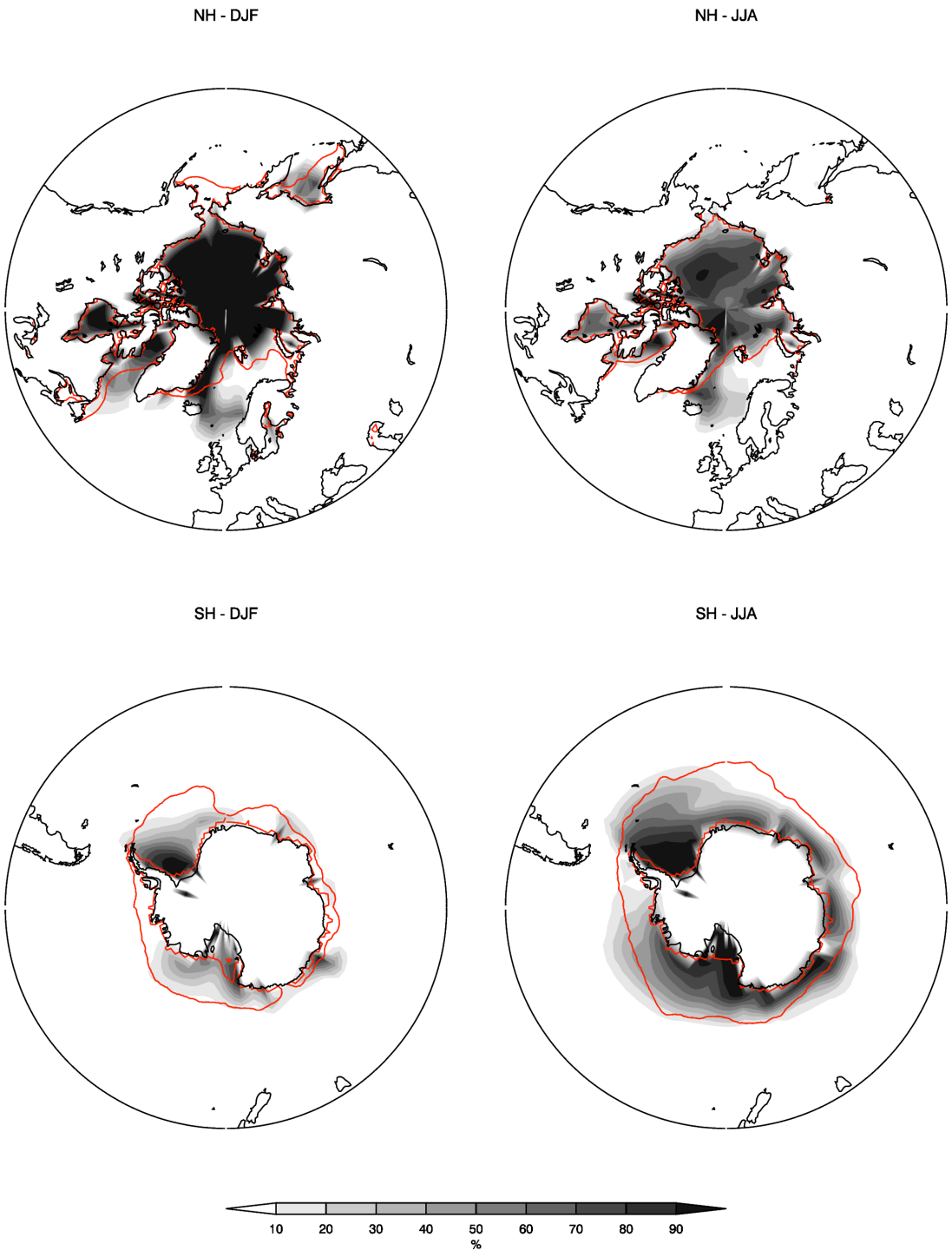

Figure 12: Fractional sea-ice extent. HadISST v1.1 15% observed contour plotted in red.

4. Simulation of ENSO

Numerous ENSO inter comparison projects have been performed with AOGCMs that find coupled GCMs ability to simulate ENSO is improving yet there are many areas that would benefit from further improvements. In most cases the models do not accurately capture the ocean-atmosphere dynamics of ENSO when compared to the observed record. AchutaRao and Sperber (2002, herein referred to as AS02) compared simulations from the 17 models that were used in Coupled Model Intercomparison Project (CMIP). AchutaRao and Sperber (2006, herein referred to as AS06) published a follow-up paper to assess whether the models used in IPCC AR4 performed better than the prior generation of CMIP models evaluated in AS02. In this section we seek to apply the techniques used in AS02 and AS06 to the simulation of ENSO using GENMOM.

a. Validation datasets

To evaluate ENSO in GENMOM, we use NOAA NCEP Reanalysis 1 (NCEP1, Kalnay et al., 1996) as opposed to NCEP2, which is significantly shorter in length. The NCEP1 data spans 1948 – 2007 providing a relatively long ENSO record. Because NCEP1 relies on a global reanalysis model, the Hadley Ice and Sea Surface Temperature v1.1 (HadISST) dataset is used in conjunction with the NCEP1 data to provide observed SSTs. Unlike AS02 and AS06, which uses the HadISST data for 1871 - 1999, we restrict the HadISST dataset to the time period of NCEP1 (1948 - 2007).

Here we compare a subset period of 60 years from the 600-year GENMOM simulation to the observed records (model years 640-699). The 60-year period was chosen by dividing the 600-year record into 10 non-overlapping intervals and calculating the standard deviation of the Niño 3 index for each period. We then selected the 60-year

period that had a Niño 3 index standard deviation closest to that of HadISST (see section 4d. for Niño index definition). Eight selected IPCC AR4 models are included for context. The time period analyzed for each of these comparison models is the last 60 years of the Climate of the 20th Century experiment.

b. Simulated tropical Pacific

In general, much of the equatorial tropical Pacific Ocean in GENMOM has a cold bias of ~2°C. Warm water anomalies, caused by a weakened South Pacific Gyre, are indicated west of South America. Figure 13 shows Hovmöller plots of the seasonal evolution of SST over the tropical Pacific for both observed and model simulated. On a seasonal basis, the simulated evolution of SST from GENMOM has similar characteristics to the IPCC AR4 models shown. Few of the IPCC AR4 models shown produce the observed range of temperatures and only GENMOM has a noticeable semi-annual cycle. GENMOM produces the warm winter anomalies further east than the observations, which causes a stronger than observed variability in the western Pacific.

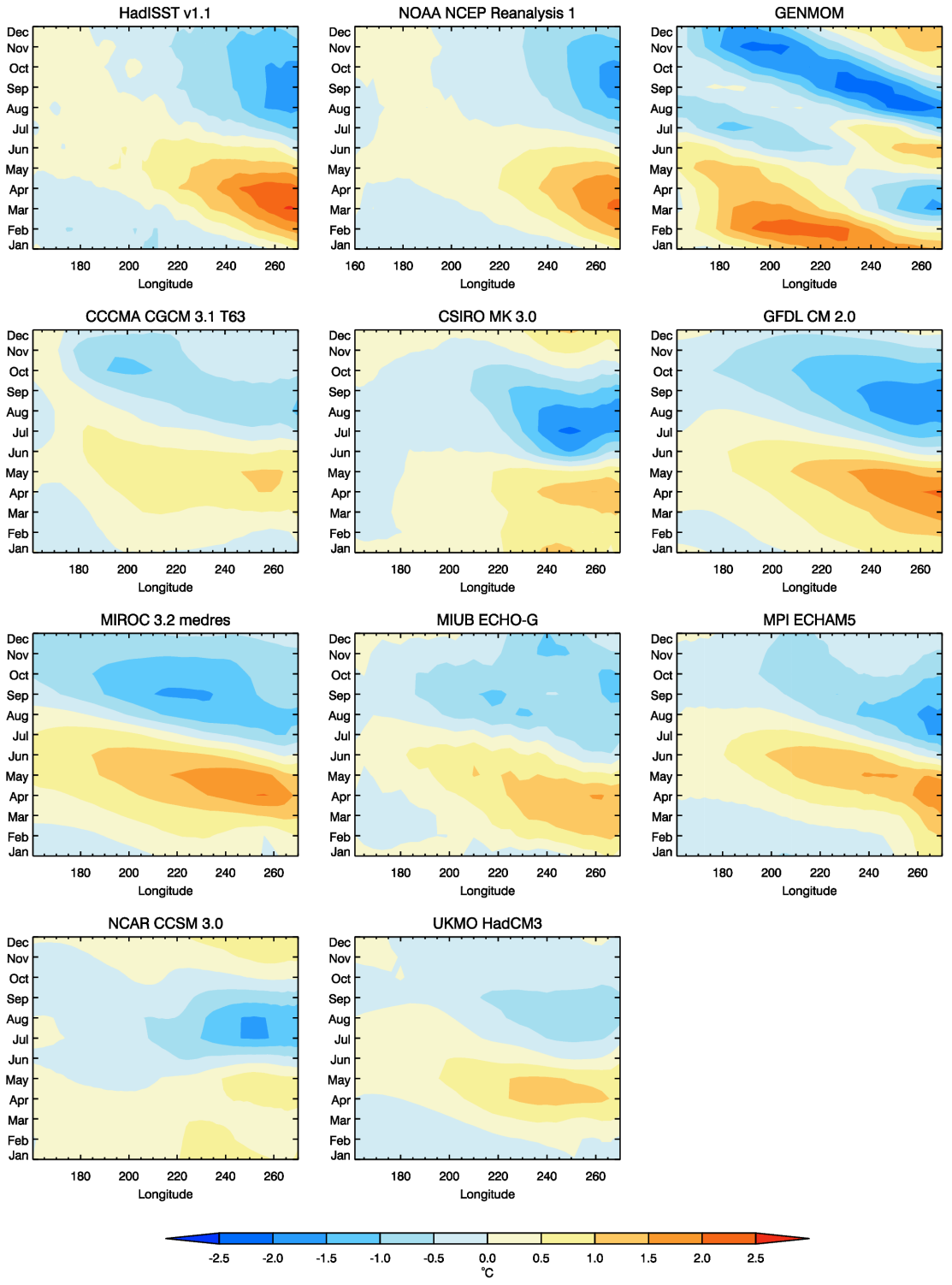

Figure 13: Evolution of the seasonal cycle of surface air temperature (2 m) for the Pacific basin for observations, GENMOM and 8 IPCC AR4 models. The seasonal temperature cycle per grid cell between 5N and 5S is calculated as the monthly deviation from the annual average.

c. ENSO regions of variability

The established regions in the tropical Pacific that are used to evaluate ENSO are: Niño 3 (5°N – 5°S, 150°W – 90°W), Niño 3.4 (5°N – 5°S, 170°W – 120°W) and Niño 4 (5°N – 5°S, 160°E – 150°W). The Niño indices are used as a metric of ENSO variability. The standard deviation of 2 m air temperature for GENMOM (full 600 years), observations (HadISST is shown as SST) and all IPCC AR4 models for these respective regions are shown in Figure 14. There is substantial spread among the IPCC AR4 models, with many models either over or under predicting the variability in the Niño 3 region. GENMOM over predicts temperature variability in the western Niño 4 and Niño 3.4 regions and under predicts in the eastern Niño 3 region. Similar to many other non flux-corrected models, GENMOM incorrectly produces peak variability in the Niño 3.4 region rather than the correct Niño 3 region. Although the region of peak variability is incorrectly simulated, the overall magnitude of variability is well simulated. The GENMOM simulated air temperature standard deviation in the Niño 3 region falls between NCEP1 and HadISST.

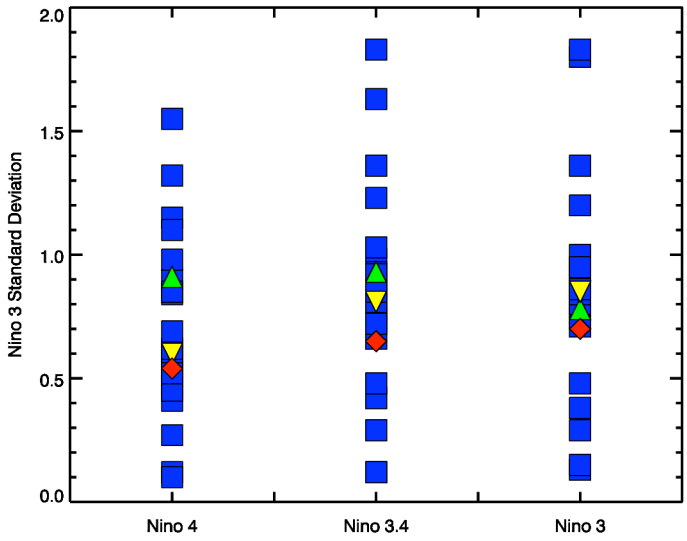

Figure 14: Standard deviations of surface air temperature (2 m) for observed, IPCC AR4 models and GENMOM for the Niño regions. GENMOM (green), HadISST (yellow), and NCEP1 (red). HadISST is shown as SST rather than 2 m air temperature. IPCC model results are provided in Table 2 of AchutaRao and Sperber (2006).

d. ENSO time series

The ENSO index is calculated as monthly SST deviations from the climatological monthly mean. The definition of an El Niño (La Niña) event is when the index remains above (below) 0.5°C (-0.5°C) for six consecutive months using a five month smoothed time series (Trenberth, 1997). The GENMOM SST time series (model years 640-699) for the Niño 3 region displays irregular amplitudes that are generally lower in magnitude than those of either the two observed datasets (Fig. 15). The attenuated amplitude is consistent with the nature of the standard deviation values (Fig. 14). The Niño 3 index is well simulated in GENMOM, even at T31 resolution. The 600-year simulation of the Niño 3 index displays essentially symmetrical amplitude of warm and cold events, rather than being skewed towards warm events as is the case in the observed record.

The spectra of the simulated Niño 3 index computed by the Maximum Entropy Method (MEM, AS02, AS06) displays a single peak at 6.1 years. In contrast, the NCEP1 and HadISST v1.1 time series display peak power at 3.9 and 4.3 years respectively (Fig. 16). The ENSO produced by GENMOM is less frequent than those for observed ENSO, but the broad spectral peak is similar to the observations. (Broad spectral peaks indicate that ENSO events are occurring at irregular intervals between 4 and 8 years.) Many of the IPCC AR4 models produce ENSO events that are too frequent and too regular, which are indicated by narrow peaks in the power spectra (AS06 Fig. 2a). Significant spectral peak in the 2 - 7 year range is absent in most of the IPCC AR4 models. A few of the IPCC AR4 models do not produce enough variability in the Niño 3 region with the magnitude of the anomalies greater than ± 0.5°C for six consecutive months, thereby failing to meet the criterion for an ENSO event.

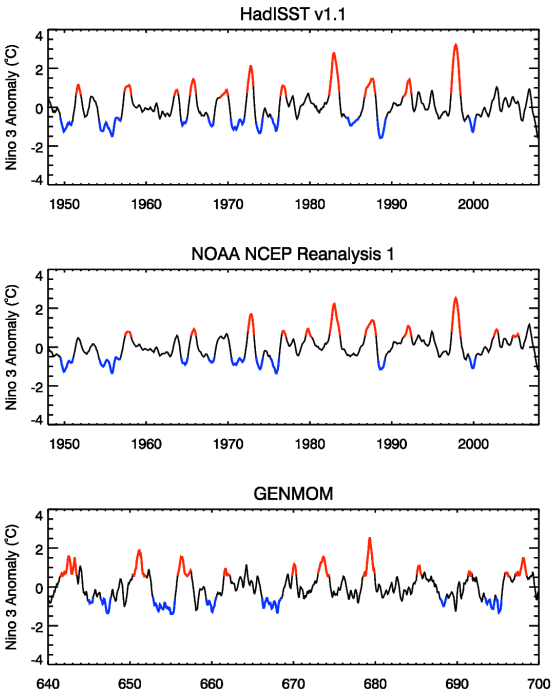

Figure 15: Observed and simulated Niño 3 indices.

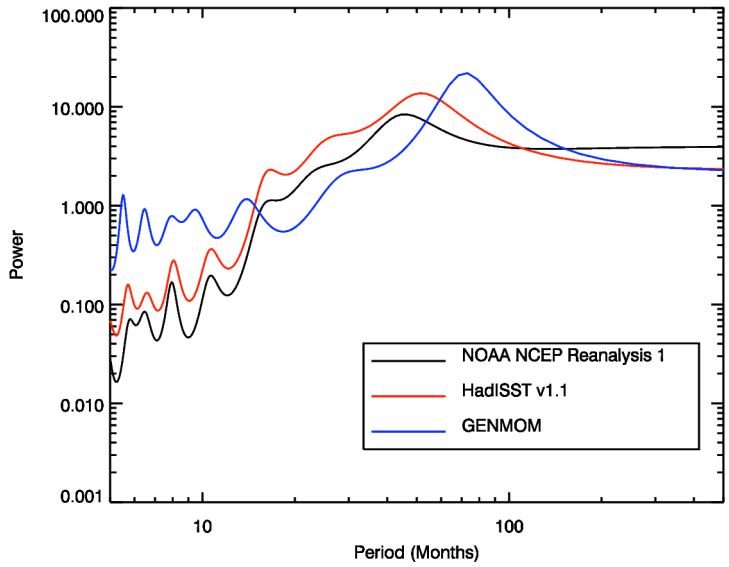

Figure 16: Observed and simulated Niño 3 index MEM spectra. The SSA Toolkit (Dettinger et al., 1995) was used to calculate power spectra via the Maximum Entropy Method.

e. Composites of ENSO events

ENSO composites are created by globally averaging all DJF periods wherein ENSO events occur. During warm El Niño events the warm tongue of SST in the tropical Pacific and the realted global teleconnections expressed as temperature and precipitation anomalies are generally well simulated (Fig. 17 and Fig. 18). The warm tongue is too confined to the equator, which is similar to a few of the IPCC AR4 models. The width of the GENMOM simulated warm tongue is similar to the observations. Some models, such as CISRO MK 3.0, simulate a warm tongue that is too wide, while others, such as MIUB ECHO-G, simulate a narrow warm tongue. The classic horseshoe-shaped pattern of cold anomalies surrounding the warm tongue is well simulated in GENMOM. The cold SST anomalies associated with the strengthening of the Aleutian Low during an El Niño are not well simulated in GENMOM, which is a common deficiency in the IPCC AR4 models.

The cold La Niña events simulated by GENMOM have similar characteristics to the warm events, such as a cold tongue with the correct width but that is too confined to the equator. Similar to warm events, the subtropical high in the Pacific is strengthened during cold events in the observed data, but this feature is not well captured by any of the models. GENMOM has the unique feature of warming over parts of the northern pole during cold events, which is not seen in the other IPCC AR4 models. Figures 17 and 18 suggest that the models with the highest resolution do not necessarily produce the most realistic ENSO pattern. ECHO-G has the lowest resolution, which is similar to GENMOM, yet it arguably produces the best spatial pattern.

During an El Niño event, warm surface waters along the equator in the Pacific are pushed east, which results in a corresponding eastward shift in rain pattern (Fig. 19). The simulation of this eastward shift in GENMOM is too weak. GENMOM incorrectly simulates drying in the Indian Ocean during DJF of El Niño events. During La Niña events, GENMOM simulates similar spatial patterns in the tropics to the observations, albeit with a stronger magnitude along the equator (Fig. 20). All of the models shown, including GENMOM, fail to adequately capture the intensity of the observed mid-latitude teleconnections associated with La Niña. GENMOM simulates increased rainfall across both eastern and western coasts of North America during El Niño events, along with decreased precipitation across both coasts during La Niña events. Although the pattern of these teleconnections are correct, the magnitude of the North American precipitation teleconnection is weaker-than-observed in the western coast.

The spatial pattern of ENSO teleconnections over North America is important for further regional downscaling and deserves additional attention here. GENMOM simulates the warm-cold dipole during El Niño events over North America and Canada well. Of the eight IPCC AR4 models shown here, only two adequately capture this temperature dipole. During cold La Niña events, the temperature dipole is reversed with warm anomalies in the southeast United States and cold anomalies over Canada. Again, GENMOM simulates this reversal well with the exception that Alaska has the opposite anomaly sign. Of the eight models shown, only two correctly simulate the La Niña temperature dipole over North America.

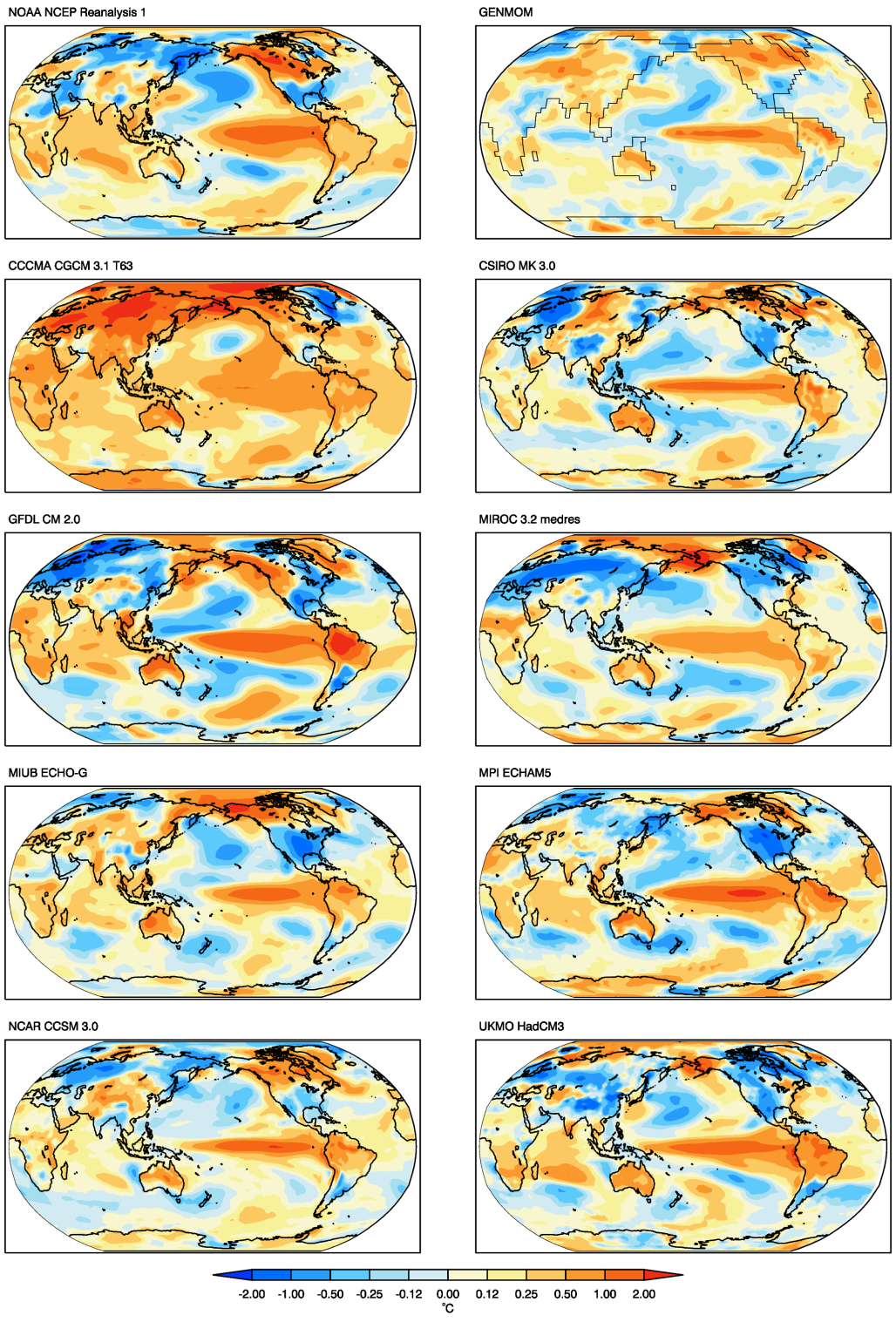

Figure 17: Surface air temperature (2 m) DJF El Niño composite anomalies for observed, 8 IPCC AR4 models and GENMOM. Both GENMOM and IPCC AR4 models are averaged over a 60-year period.

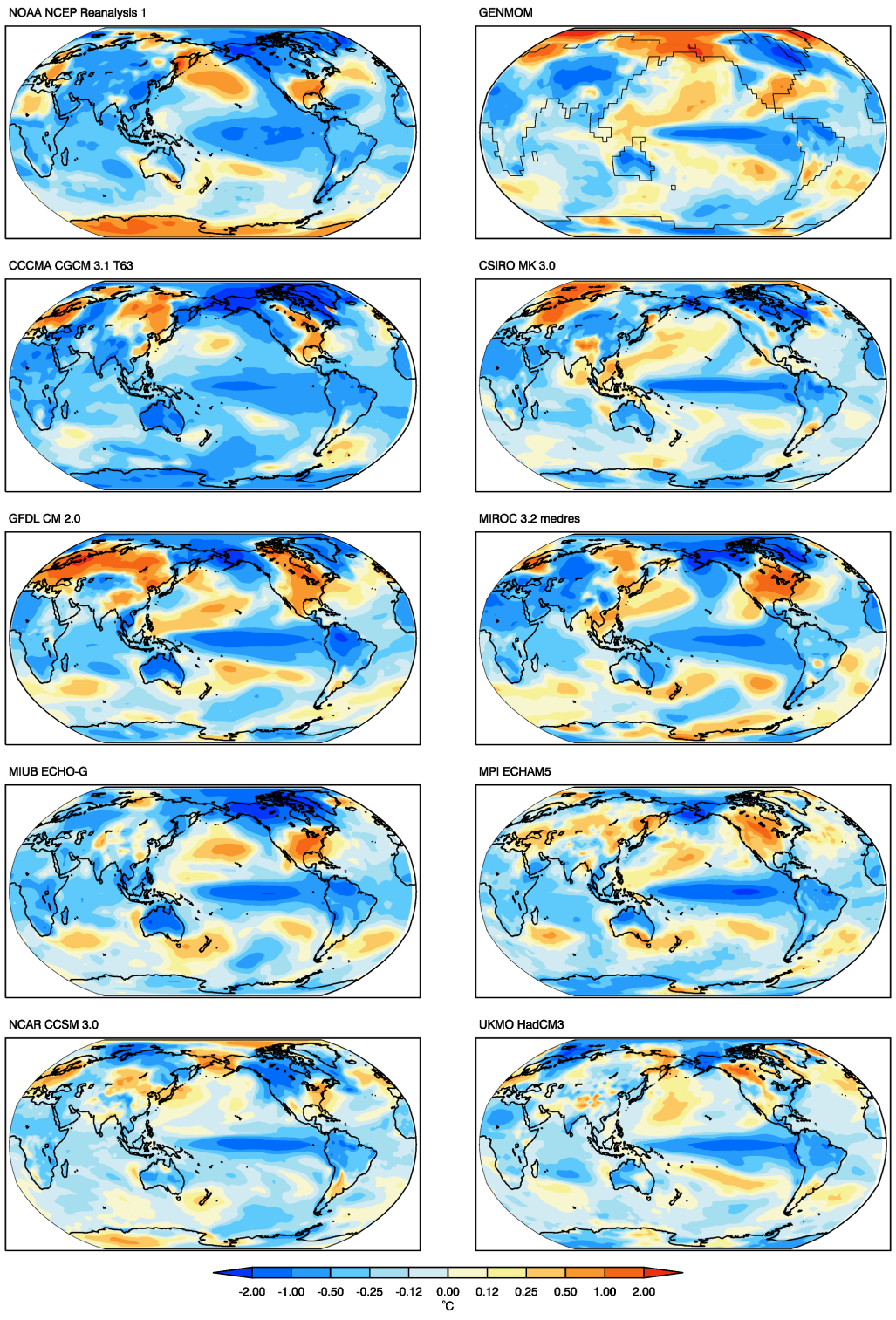

Figure 18: Surface air temperature (2 m) DJF La Niña composite anomalies for observed, 8 IPCC AR4 models and GENMOM. Both GENMOM and IPCC AR4 models are averaged over a 60-year period.

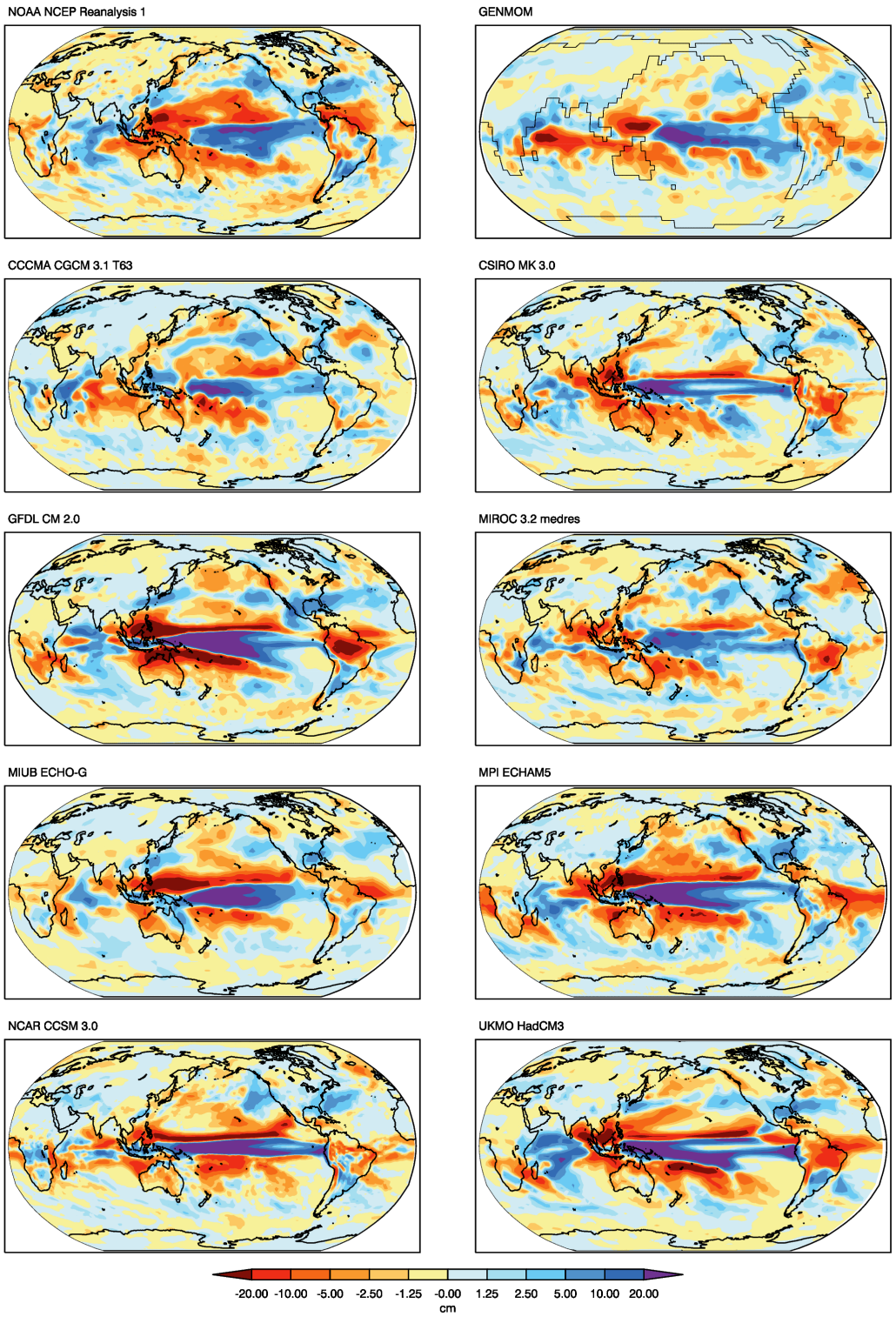

Figure 19: Precipitation DJF El Niño composite anomalies for observed, 8 IPCC AR4 models and GENMOM. Both GENMOM and IPCC AR4 models are averaged over a 60-year period.

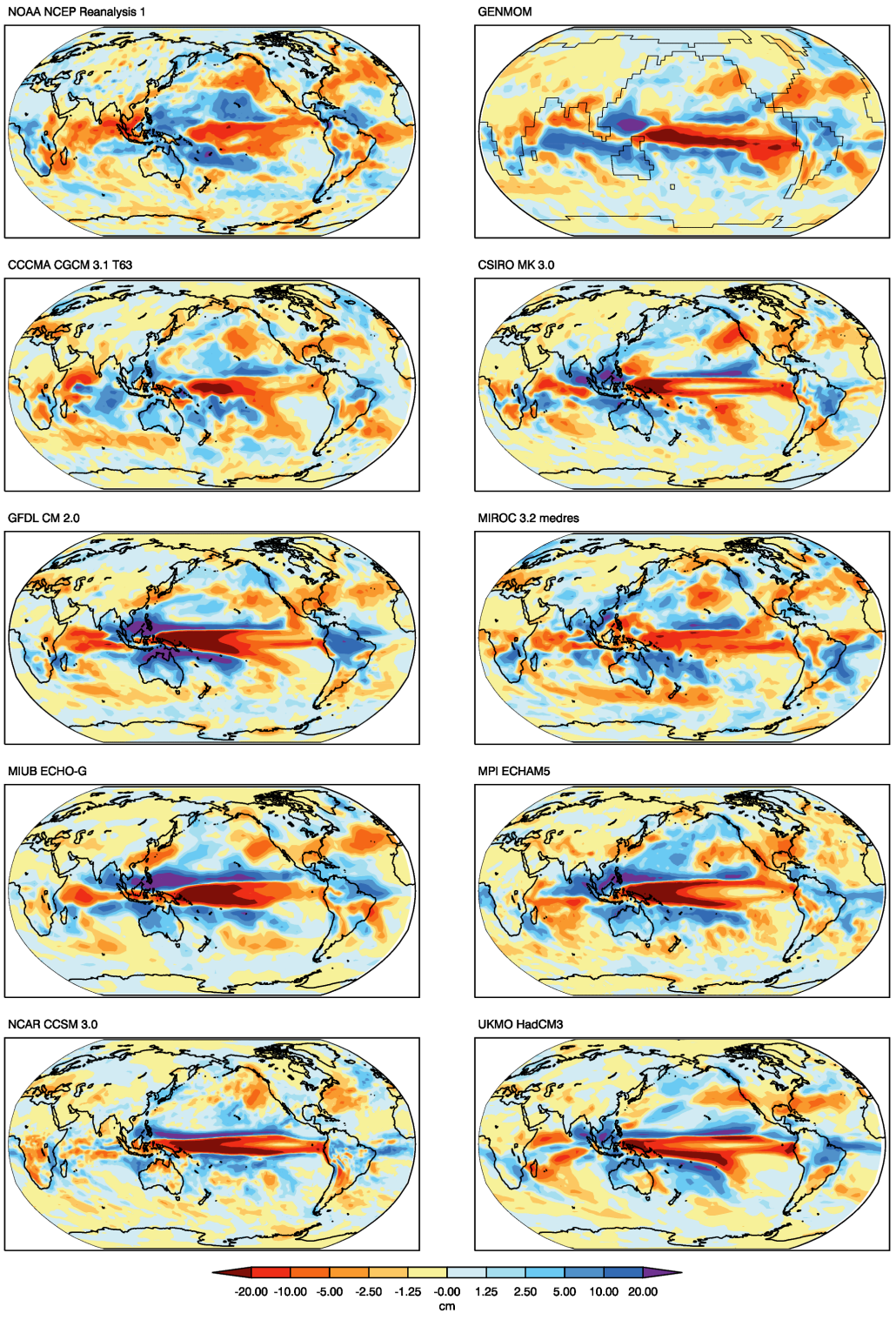

Figure 20: Precipitation DJF La Niña composite anomalies for observed, 8 IPCC AR4 models and GENMOM. Both GENMOM and IPCC AR4 models are averaged over a 60-year period.

5. Changes in ENSO with global warming

In this section we detail the response of ENSO to present day, doubling (710 ppmV) and quadrupling (1420 ppmV) of atmospheric CO_2 (hereafter denoted 1x, 2x and 4x respectively). The three simulations are integrated for 1,000 years. The first 400 years are disregarded in this analysis. Other trace gases such as CH_4 and N_2O were not altered from 1x values. The most dramatic warming occurs at the poles during winter (Fig. 21), which is caused by a change in the ice-albedo feedback due to reduced sea-ice distributions in the warming scenarios (not shown). All models simulate warming along the equatorial Pacific, which potentially may affect ENSO. Generally, GENMOM has a similar spatial distribution of sensitivity to CO_2 warming when compared to the IPCC AR4 models. GENMOM has a global equilibrium sensitivity of 2.3°C, which compares well to the equilibrium sensitivity of 2.1°C - 4.4°C reported in the IPCC AR4 (Meehl et al., 2007). However, GENMOM has a more moderate warming at the North Pole and more intense warming at the South Pole than other models, which is due to differing responses of sea-ice to warming in the models.

The Niño 3 indices for all three simulations are shown in Figure 22; increased variability with CO_2 levels is readily apparent. The standard deviation of 1x, 2x and 4x are 0.78, 0.89, and 0.96 respectively, indicating that GENMOM simulates increasing variability in the Niño 3 region with global warming. Based on F-tests, the time series are found to have statistically significantly different variance at the 95% confidence level ($\sigma = 0.05$). MEM Spectral analysis of the time series (not shown) reveals periods of 5.3, 5.0 and 4.5 years for 1x, 2x, and 4x, indicating that GENMOM also simulates more frequent ENSO events with increasing CO_2-dependent global warming. Potential causes

for the increased ENSO amplitude could be changes in the strength of the tropical thermocline or the meridional extent of the zonal wind stress response to anomalous equatorial SST (Merryfield, 2006). The leading proposed mechanism for a decreased ENSO period with global warming is that the rate at which Kelvin and Rosby waves propagate across the Pacific basin increases as the water temperature increases (Chelton et al., 1998, Merryfield, 2006). Kelvin and Rosby waves are thought to be associated with the triggering of ENSO events. If the waves propagate quicker across the Pacific Basin, then the frequency of ENSO events would consequent increase.

An additional noteworthy feature of the Niño 3 indices presented in Figure 22 is presence of multi-decadal modulation of ENSO amplitude. Modulation of ENSO amplitude can be identified in the time series as pulses of periods with high ENSO variability followed by periods of low variability. Similar modulation can readily be seen in model years 600 - 700 in the 2x time series. Wavelet and spectral analysis of this low frequency component suggests that it does not appear to have a preferred frequency because the spectra has very little power. Discussion on multi-decadal modulation of ENSO amplitude can be found in Timmermann (2003), Yeh and Kirtman (2004), and Lin (2007).

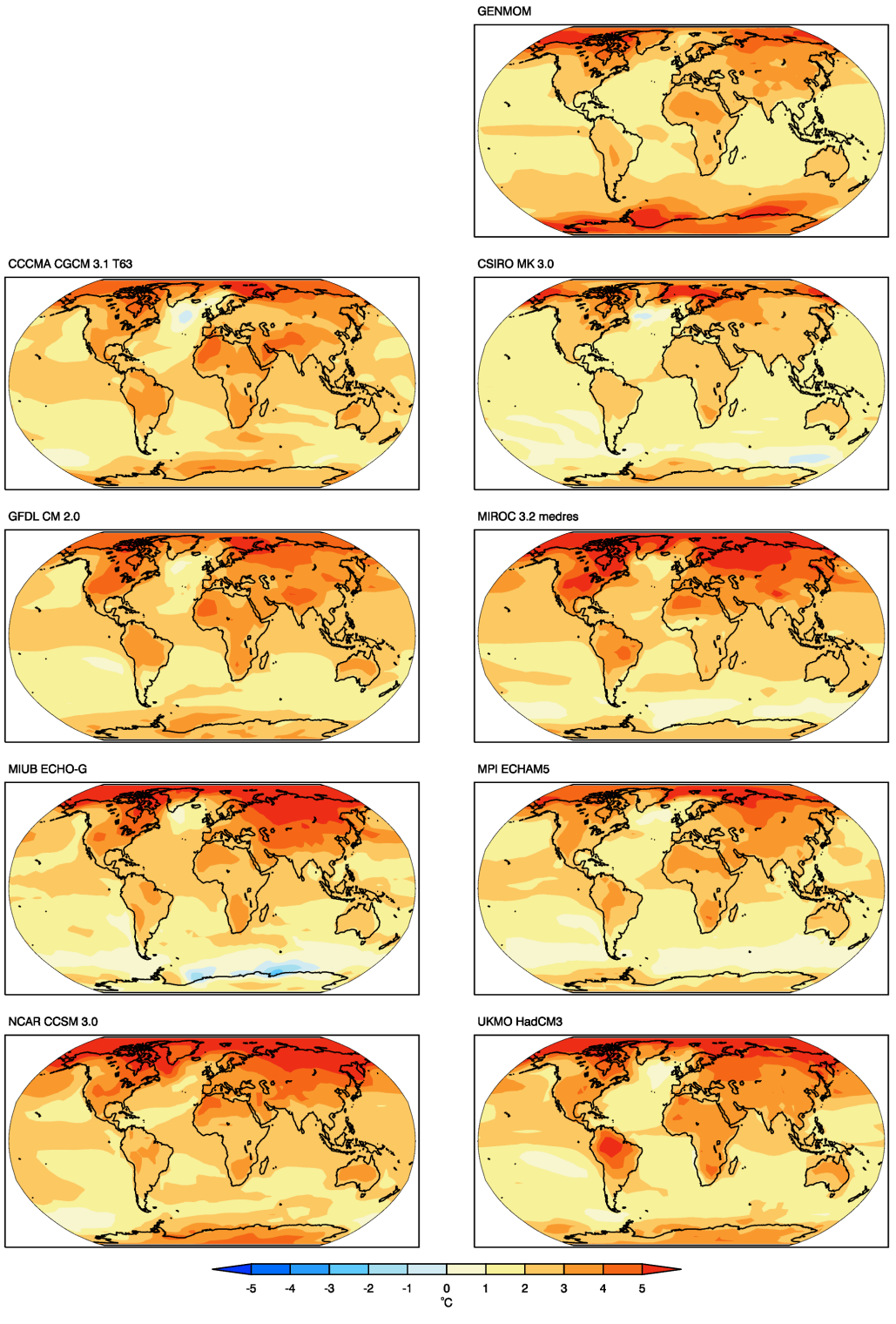

Figure 21: AOGCM sensitivity to a doubling of CO_2 for 8 IPCC AR4 models and GENMOM. GENMOM anomalies are calculated as the last 30 years of 2x equilibrium simulation minus the last 30 years of 1x equilibrium simulation. IPCC anomalies are calculated as the 30 years surrounding double CO_2 in the SRES A2 emission scenario minus the last 30 years of the Climate of the 20th Century experiment.

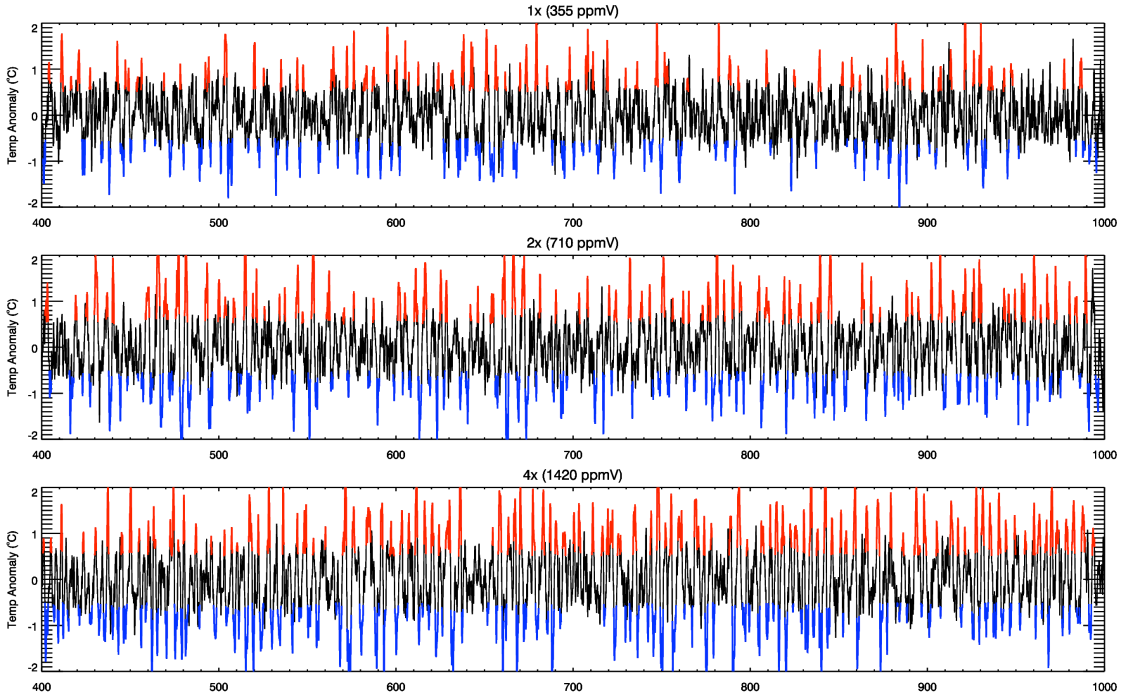

Figure 22: GENMOM simulated Niño 3 index for 1x, 2x and 4x with El Niño (red) and La Niña (blue) events highlighted.

6. Concluding remarks

Here we have presented the first formal evaluation of the new AOGCM, GENMOM, which is a non-flux corrected model comprised of GENESIS 3 atmospheric model, MOM2 ocean model and LSX. The main changes in GENESIS version 3 are (i) solar and thermal infrared radiation are calculated using the NCAR CCM3 radiation code, and (ii) the ocean is optionally represented by the MOM2 ocean general circulation model. The spectral resolution of T31 for both atmosphere and ocean is used during this evaluation.

The GENMOM present-day simulation is evaluated with comparisons with NCEP2 and OI SST. The land mask, topography, bathymetry and ice sheet extent is derived from the ICE-4G dataset. The global temperature is below observed, indicating a small global cold bias (0.7°C); which has a warm bias over ocean (0.2°C) and a cold bias over land (1.0°C). The annual surface temperature gradient and spatial distribution compare well to both observations and to the IPCC AR4 models. Cold SST anomalies in the Norwegian Sea are explained by excessive sea-ice in both winter and summer. One noticeable feature in the surface temperature field is a warm bias in the Southern Ocean with a larger than observed seasonal cycle. This is attributed to a mid-depth ocean warm temperature bias in the tropics that then propagates to the surface in the Southern Ocean. A warm bias in the ocean mid-layers may be due to a failure in ocean circulation or weaker-than-observed ocean heat transport. GENMOM fails to resolve adequately the South Pacific Gyre, which results in a warm SST bias in the eastern Pacific as well as a failure to simulate the corresponding anticyclonic atmospheric circulation around the gyre. Atmospheric fields such as the jet stream structure and major MSLP features are

well simulated. Precipitation patterns are improved in comparison to previous versions of GENESIS. GENESIS simulates a distinct double ITCZ when coupled with the OGCM. Sea-ice is well simulated with the exceptions of excess sea-ice in the Norwegian Sea and deficient sea-ice in Antarctica during summer. The evaluation performed here has shown that GENMOM produces a realistic climatology that is comparable to the models used in the IPCC AR4. GENMOM shares similar deficiencies with other models such as a double ITCZ, failure to resolve features due to resolution limitations (the California and Humboldt Currents), and having a global cold bias.

GENMOM produces a realistic ENSO that is of similar quality to the eight IPCC AR4 models evaluated here. The mean state of surface temperature is offset towards the west and produces a semiannual seasonal cycle that is not seen in the select IPCC AR4 models evaluated here. However, the seasonal temperature range is well simulated and close to the observed range. GENMOM incorrectly produces peak ENSO variability in the Niño 3.4 region as opposed to the correct Niño 3 region. The GENMOM simulated ENSO amplitude is bound between the NCEP1 and HadISST values. The simulated ENSO period of 5.3 yr (model years 400-999) is longer than the observed 4.3 year period, but still places GENMOM among the best of the IPCC AR4 models.

The spatial fingerprint of surface temperatures associated with ENSO events for in GENMOM is both similar to the observations and comparable with the IPCC AR4 models. The GENMOM simulated tropical Pacific precipitation patterns compare well to observations at the tropics but are inadequate in mid-latitudes. GENMOM produces a precipitation teleconnection to the Indian Ocean of the incorrect sign in both warm and cold events. In the context of regional downscaling in North America, GENMOM

simulates both temperature and precipitation ENSO teleconnections to North America similar to observations, which is not captured by many of the IPCC AR4 models evaluated here.

Long (600-year) CO_2 sensitivity experiments show that GENMOM simulates more frequent and higher amplitude ENSO events with CO_2-dependent global warming. This result should be interpreted with caution as the IPCC AR4 indicates that models show no consensus on how ENSO will respond to global warming. The IPCC AR4 models are divided between a more intense ENSO and a damped ENSO in response to global warming. These issues stress the need for a multi-model approach in applying the results of climate models to business and political decisions.

A next step in validating the findings here would be to perform equally long CO_2 sensitivity experiments with other IPCC models. In many cases, the current IPCC 2x CO_2 simulations are simply too short to allow statistical validation of potential changes in ENSO with global warming. Moreover, models that exhibit a multi-decadal modulation of ENSO amplitude require even longer simulations because it becomes difficult to separate a CO_2 forced change in ENSO from the modulation. Many of the modeling groups using more complex, higher resolution models included in the IPCC AR4 may find it difficult to perform long simulations due to computational and time limitations. Moreover, longer perpetual CO_2 simulations are not a priority in the IPCC assessment roadmap, as transient CO_2 simulations are more realistic of possible future emission scenarios.

References

AchutaRao, K. and K. R. Sperber, 2002: Simulation of the El Niño Southern Oscillation: Results from the Coupled Model Intercomparison Project. Climate Dyn., 19, 191–209.

AchutaRao, K. and K. R. Sperber, 2006: ENSO simulation in coupled ocean-atmosphere models: Are the current models better? Climate Dynamics, 10.1007/s00382-006-0119-7.

Anthes, R.A., 1977: A cumulus parameterization scheme utilizing a one-dimensional cloud model. Mon. Wea. Rev. 105, 270-286.

Beckmann, B., S. Floegel, P. Hoffman, M. Schulz and T. Wagner, 2005: Orbital forcing of Cretaceous river discharge in tropical Africa and ocean response. Nature, 437, 241-244.

Bice, K.L., D. Birgel, P.A. Meyers, K.A. Dahl, K.-U. Hinrichs and R.D. Norris, 2006: A multiple proxy and model study of Cretaceous upper ocean temperatures and atmospheric CO2 concentrations. Palaeoceanography, 21, PA2002, doi:10.1029/2005PA001203, 1-17.

Bryan, K., 1969: A numerical method for the study of the circulation of the world oceans. J. Comput. Phys., 4, 347–376.

Chelton, D. B., R. A. deSzoeke, M. G. Schlax, K. El Naggar, and N. Siwertz, 1998: Geographical variability of the first baroclinic Rossby radius of deformation. J. Phys. Oceanogr., 28, 433–460.

Clapp, R.B., and G.M. Hornberger, 1978: Empirical equations for some soil hydraulic properties. Water Res. Res., 14, 601-604.

Clement, A. C., R. Seager, and M. A. Cane, 1999: Orbital controls on the El Niño/Southern Oscillation and the tropical climate, Paleoceanography, 14, 441 – 456.

Collins, M., 2000a: Uncertainties in the response of ENSO to Greenhouse Warming, Geophys. Res. Lett., 27, 3509–3513.

Collins, M., 2000b: The El-Niño Southern Oscillation in the second Hadley Centre coupled model and its response to greenhouse warming. J. Climate, 13, 1299–1312.

Collins, W.D., et al., 2004: Description of the NCAR Community Atmosphere Model (CAM3.0). Technical Note TN-464+STR, National Center for Atmospheric Research, Boulder, CO, 214 pp.

DeConto, R.M., D. Pollard and D. Harwood, 2006: Sea ice feedback and Cenozoic evolution of Antarctic climate and ice sheets. Paleoceanography, 22, PA3214, doi:10.1029/2006PA001350.

DeConto, R.M., D. Pollard, P. Wilson, H. Palike, C. Lear and M. Pagani, 2008: Thresholds for Cenozoic bipolar glaciation. Nature, 455, 653-656.

Dettinger MD, Ghil M, Strong CM, Weibel W, Yiou P, 1995: Software expedites singular-spectrum analysis of noisy time series. Eos 76: 12

Dickinson, R.E., 1984: Modeling evapotranspiration for three-dimensional global climate models. In: Hansen, J.E. and Takahashi, T. (eds.), Climate Processes and Climate Sensitivity. Geophysical Monograph 29, American Geophysical Union, Washington D.C., 58-72.

Flato, G.M., 2005: The Third Generation Coupled Global Climate Model (CGCM3) (and included links to the description of the AGCM3 atmospheric model). http://www.cccma.bc.ec.gc.ca/models/cgcm3.shtml.

Flato, G.M., and W.D. Hibler., 1992: Modeling pack ice as a cavitating fluid. J. Phys. Oceanogr., 22, 626-651.

GFDL GAMDT (The GFDL Global Atmospheric Model Development Team), 2004: The new GFDL global atmosphere and land model AM2- LM2: Evaluation with prescribed SST simulations. J. Clim., 17, 4641– 4673.

Giannini, A., J. C. H. Chiang, M. A. Cane, Y. Kushnir, and R. Seager, 2001: The ENSO teleconnection to the tropical Atlantic Ocean: Contributions of the remote and local SSTs to rainfall variability in the tropical Americas. J. Clim.,14, 4530 – 4544.

Gnanadesikan, A., et al., 2004: GFDL's CM2 global coupled climate models–Part 2: The baseline ocean simulation. J. Clim., 19, 675–697.

Gordon, C., et al., 2000: The simulation of SST, sea ice extents and ocean heat transports in a version of the Hadley Centre coupled model without flux adjustments. Clim. Dyn., 16, 147–168.

Gordon, H.B., et al., 2002: The CSIRO Mk3 Climate System Model. CSIRO Atmospheric Research Technical Paper No. 60, Commonwealth Scientific and Industrial Research Organisation Atmospheric Research, Aspendale, Victoria, Australia, 130 pp, http://www.cmar.csiro.au/e-print/ open/gordon_2002a.pdf.

Harvey, L.D.D., 1988: Development of a sea ice model for use in zonally averaged energy balance climate models. J. Climate, 1, 1221-1238.

Horel, J. D., and J. M. Wallace, 1981: Planetary-scale atmospheric phenomena associated with the Southern Oscillation. Mon. Wea. Rev., 109, 813–829.

Horton, D.E., C.J. Poulsen and D. Pollard, 2007: Orbital and CO2 forcing of late Paleozoic continental ice sheets. Geophys. Res. Lett., 34, L19708, doi:10.1029/2007GL031188.

Hostetler, S.W., Giorgi, F. 1995: Effects of a 2xCO2 climate on two large lake systems: Pyramid Lake, Nevada, and Yellowstone Lake, Wyoming. Global and Planetary Change 10: 43–54.

Hostetler, S.W., P.J. Bartlein, P.U. Clark, E.E. Small, A.M. Solomon, 2000: Simulated influences of Lake Agassiz on the climate of central North America 11 000 years ago. Nature 405: 334–337.

Hostetler, S.W., N.J. Pisias, and A.C. Mix, 2006: Sensitivity of Last Glacial Maximum climate to uncertainties in tropical and subtropical ocean temperatures. Quat. Sci. Rev., 25, 1168-1185.

Joussaume, S., K.E. Taylor , P. Braconnot, J.F.B. Mitchell, J.E. Kutzbach, S.P. Harrison, I.C. Prentice, A.J. Broccoli, A. Abe-Ouchi, P.J. Bartlein, C. Bonfils, B. Dong, J. Guiot, K. Herterich, C.D. Hewitt, D. Jolly, J.W. Kim, A. Kislov, A. Kitoh, M.F. Loutre, V. Masson, B. McAvaney, N. McFarlane, N. de Noblet, W.R. Peltier, J.Y. Peterschmitt, D.

K-1 Model Developers, 2004: K-1 Coupled Model (MIROC) Description. K-1 Technical Report 1 [Hasumi, H., and S. Emori (eds.)]. Center for Climate System Research, University of Tokyo, Tokyo, Japan, 34 pp., http://www.ccsr.u-tokyo.ac.jp/kyosei/hasumi/MIROC/tech-repo.pdf.

Kalnay, E. et al. The NCEP/NCAR 40-year reanalysis project, 1996: Bull. Am. Meteorol. Soc. 77, 437 - 471.

Lin, J. L., 2007: The double-ITCZ problem in IPCC AR4 coupled GCMs: Ocean–atmosphere feedback analysis. J. Climate, 20, 4497–4525.

Lin, J.L., 2007: Interdecadal variability of ENSO in 21 IPCC AR4 coupled GCMs, Geophys. Res. Lett., 34: L12702, doi:10.1029/2006GL028937.

Liu, Z., J. Kutzbach, and L. Wu, 2000: Modeling climate shift of El Nino variability in the Holocene, Geophys. Res. Lett., 27, 2265 – 2268.

Locarnini, R. A., A. V. Mishonov, J. I. Antonov, T. P. Boyer, and H. E. Garcia, 2006: World Ocean Atlas 2005, Volume 1: Temperature. S. Levitus, Ed. NOAA Atlas NESDIS 61, U.S. Government Printing Office, Washington, D.C., 182 pp.

NCEP-DEO AMIP-II Reanalysis (R-2): M. Kanamitsu, W. Ebisuzaki, J. Woollen, S-K Yang, J.J. Hnilo, M. Fiorino, and G. L. Potter, 2002: Bul. of the Atmos. Met. Soc, 1631-1643.

Kalnay, E., M. Kanamitsu, R. Kistler, W. Collins, D. Deaven, L. Gandin, M. Iredell, S. Saha, G. White, J. Woollen, Y. Zhu, A. Leetmaa, B. Reynolds, M. Chelliah, W. Ebisuzaki, W. Higgins, J. Janowiak, K. C. Mo, C. Ropelewski, J. Wang, R. Jenne, and D. Joseph, 1996: The NCEP/NCAR 40-Year Reanalysis Project. Bulletin of the American Meteorological Society.

Kiehl, J.T., J.J. Hack, G.B. Bonan, B.A. Boville, D.L. Williamson and P.J. Rasch, 1998: The National Center for Atmospheric Research Community Climate Model: CCM3. J. Climate, 11, 1131-1149.

Kreitzberg, C.W., and D.J. Perkey, 1976: Release of potential instability: Part I. A sequential plume model within a hydrostatic primitive equation model. J. Atmos. Sci., 33, 456-475.

Kump, L.R. and D. Pollard, 2008: Amplification of Cretaceous warmth by biological cloud feedbacks. Science, 320, 195.

Marsland, S.J., et al., 2003: The Max-Planck-Institute global ocean/sea ice model with orthogonal curvilinear coordinates. Ocean Modelling, 5, 91–127.

McFarlane, N.A., G.J. Boer, J.-P. Blanchet, and M. Lazare, 1992: The Canadian Climate Centre second-generation general circulation model and its equilibrium climate. J. Clim., 5, 1013–1044.

Meehl, G.A., T.F. Stocker, W.D. Collins, P. Friedlingstein, A.T. Gaye, J.M. Gregory, A. Kitoh, R. Knutti, J.M. Murphy, A. Noda, S.C.B. Raper, I.G. Watterson, A.J. Weaver and Z.-C. Zhao, 2007: Global Climate Projections. In: Climate Change 2007: The Physical Science Basis. Contribution of Working Group I to the Fourth Assessment Report of the Intergovernmental Panel on Climate Change [Solomon, S., D. Qin, M. Manning, Z. Chen, M. Marquis, K.B. Averyt, M. Tignor and H.L. Miller (eds.)]. Cambridge University Press, Cambridge, United Kingdom and New York, NY, USA.

Merryfield, W. J., 2006: Changes to ENSO under CO2 doubling in a multimodel ensemble. J. Climate, 19, 4009–4027.

Miller, G., J. Mangan, D. Pollard, S. Thompson, B. Felzer and J. Magee, 2005: Sensitivity of the Australian monsoon to insolation and vegetation: implications for human impact on continental moisture balance. Geology, 33, 1, 65-68.

Neelin, J. D., D. S. Battisti, A. C. Hirst, F.-F. Jin, Y. Wakata,T. Yamagata, and S. E. Zebiak, 1998: ENSO theory, J. Geophys.Res., 103, 14,261–14,290.

Otto-Bliesner, B. L., E. C. Brady, S.-I. Shin, Z. Liu, and C. Shields, 2003: Modeling El Niño and its tropical teleconnections during the last glacial–interglacial cycle. Geophys. Res. Lett., 30, 2198, doi:10.1029/2003GL018553.

Pacanowski, R.C., K. Dixon, and A. Rosati, 1993: The GFDL Modular Ocean Model Users Guide, Version 1.0. GFDL Ocean Group Technical Report No. 2, Geophysical Fluid Dynamics Laboratory, Princeton, NJ.

Pacanowski, R.C., 1996: MOM 2 Version 2.0 (Beta) Documentation: User's Guide and Reference Manual. NOAA GFDL Ocean Technical Report 3.2, 329 pp.

Peltier, W. R., 2002: Global glacial isostatic adjustment: palaeogeodetic and space-geodetic tests of the ICE-4G (VM2) model. J. Quaternary Sci., Vol. 17 pp. 491–510. ISSN 0267-8179.

Pinot, S., G. Ramstein, S. P. Harrison, I. C. Prentice, J. Guiot, M. Stute, and S. Joussaume, 1999: Tropical paleoclimates at the Last Glacial Maximum: Comparison of Paleoclimate Modeling Intercomparison Project (PMIP) simulations and paleodata, Clim. Dyn., 15, 857–874.

Pollard, D., J.C. Bergengren, L.M. Stillwell-Soller, B. Felzer, and S.L. Thompson, 1998: Climate simulations for 10 000 and 6 000 years BP using the GENESIS global climate model, Paleoclimates - Data and Modelling, 2, 183-218.

Pollard, D. Rind, J.F. Royer, M.E. Schlesinger, J. Syktus, S. Thompson, P. Valdes, G. Vettoretti, R.S. Webb, and U. Wyputta, 1999: Monsoon changes for 6000 years ago: results of 18 simulations from the Paleoclimate Modeling Intercomparison Project (PMIP), Geophysical Research Letters, 26 (7), 859-862.

Pollard, D. and S.L. Thompson, 1994: Sea-ice dynamics and CO2 sensitivity in a global climate model. Atmos.-Ocean, 32, 449-467.

Pollard, D. and S.L. Thompson, 1995: Use of a land-surface-transfer scheme (LSX) in a global climate model (GENESIS): The response to doubling stomatal resistance. Global and Planetary Change, 10, 129-161.

Pope, V.D., M.L. Gallani, P.R. Rowntree, and R.A. Stratton, 2000: The impact of new physical parametrizations in the Hadley Centre climate model: HadAM3. Clim. Dyn., 16, 123–146.

Poulsen, C.J., D. Pollard and T.S. White, 2006: General Circulation Model simulation of the d18O content of continental precipitation in the middle Cretaceous: A model-proxy comparison. Geology, 35, 199-202.

Poulsen, C.J., D. Pollard, I.P. Montanez and D. Rowley, 2007: Late Paleozoic tropical climate response to Gondwanan glaciation, Geology, 35, 771-774.

Randall, D.A., R.A. Wood, S. Bony, R. Colman, T. Fichefet, J. Fyfe, V. Kattsov, A. Pitman, J. Shukla, J. Srinivasan, R.J. Stouffer, A. Sumi and K.E. Taylor, 2007: Climate Models and Their Evaluation. In: Climate Change 2007: The Physical Science Basis. Contribution of Working Group I to the Fourth Assessment Report of the Intergovernmental Panel on Climate Change [Solomon, S., D. Qin, M. Manning, Z. Chen, M. Marquis, K.B. Averyt, M.Tignor and H.L. Miller (eds.)]. Cambridge University Press, Cambridge, United Kingdom and New York, NY, USA.

Reynolds, R.W., N.A. Rayner, T.M. Smith, D.C. Stokes, and W. Wang, 2002: An Improved In Situ and Satellite SST Analysis for Climate. J. Climate, 15, 1609-1625.

Roeckner, E., et al., 1996: The Atmospheric General Circulation Model ECHAM4: Model Description and Simulation of Present-Day Climate. MPI Report No. 218, Max-Planck-Institut fü r Meteorologie, Hamburg, Germany, 90 pp.

Roeckner, E., et al., 2003: The Atmospheric General Circulation Model ECHAM5. Part I: Model Description. MPI Report 349, Max Planck Institute for Meteorology, Hamburg, Germany, 127 pp.

Ropelewski, C. F. and M. S. Halpert, 1987: Global and regional scale precipitation patterns associated with the El Niño/Southern Oscillation cycle. Mon. Wea. Rev., 115, 1606-1626.

Ruddiman, W.F., S.J. Vavrus and J.E. Kutzbach, 2005: A test of the overdue-glaciation hypothesis. Quat. Sci. Rev., 24, 1-10.

Semtner, A.J., 1976: A model for the thermodynamic growth of sea ice in numerical investigations of climate. J. Phys. Oceanogr., 6, 379-389.

Senior, C.A. and J.F.B. Mitchell, 1993: Carbon dioxide and climate: the impact of cloud parameterization. J. Climate, 6, 393-418.

Smith, R.N.B., 1990: A scheme for predicting layer clouds and their water content in a general circulation model. Q. J. Roy. Meteorol. Soc., 116, 435-460.

Smith, R.D., and P.R. Gent, 2002: Reference Manual for the Parallel Ocean Program (POP), Ocean Component of the Community Climate System Model (CCSM2.0 and 3.0). Technical Report LA-UR-02-2484, Los Alamos National Laboratory, Los Alamos, NM, http://www.ccsm. ucar.edu/models/ccsm3.0/pop/.

Smith, S. R., J. Servain, D. M. Legler, J. N. Stricherz, M. A. Bourassa, and J. J. O'Brien, 2004: Quantifying uncertainties in NCEP reanalyses using high-quality research vessel obser- vations. Bull. Amer. Meteor. Soc., 85, 979–994.

Timmermann, A., M. Latif, A. Bacher, J. Oberhuber, and E. Roeckner, 1999: Increased El Niño frequency in a climate model forced by future greenhouse warming. Nature, 398, 694-696.

Timmermann, A., 2003: Decadal ENSO amplitude modulations: A nonlinear paradigm. Global Planet. Change, 37, 135-156.

Thompson, S.L. and D. Pollard, 1995: A global climate model (GENESIS) with a land-surface-transfer scheme (LSX). Part 1: Present-day climate. J. Climate, 8, 732-761.

Thompson, S.L. and D. Pollard, 1997: Greenland and Antarctic mass balances for present and doubled CO2 from the GENESIS version 2 global climate model. J. Climate, 10, 871-900.

Trenberth, K.E., 1997: The definition of El Niño. Bulletin of the American Meteorological Society 78, 2771–2777.

Trenberth, K. E.and C. J. Guillemot, 1998: Evaluation of the atmospheric moisture and hydrological cycle in the NCEP/NCAR reanalyses. Climate Dyn., 14, 213–231.

Trenberth, K. E, D. P. Stepaniak, J. W. Hurrell, and M. Fiorino, 2001: Quality of reanalyses in the Tropics. J. Climate, 14, 1499–1510.

Williamson, D.L., and P.J. Rasch, 1989: Two-dimensional semi-Lagrangian transport with shape-preserving interpolation. Mon. Wea. Rev., 117, 102-129.

Williamson, D.L., J.T. Kiehl, V. Ramanathan, R.E. Dickinson, and J.J.Hack, 1987: Description of NCAR Community Climate Model (CCM1). NCAR Technical Note NCAR/TN-285+STR, Boulder, Colorado, 112 pp.

Wolff, J.-O., E. Maier-Reimer, and S. Lebutke, 1997: The Hamburg Ocean Primitive Equation Model. DKRZ Technical Report No. 13, Deutsches KlimaRechenZentrum, Hamburg, Germany, 100 pp., http://www.mad.zmaw.de/Pingo/reports/ReportNo.13.pdf.

Yeh, S. and B.P. Kirtman, 2004: Tropical Pacific decadal variability and ENSO amplitude modulation in a CGCM, J. Geophys. Res., 109, C11009, doi:10.1029/2004JC002442.

Zhou, J., C.J. Poulsen, D. Pollard and T.S. White, 2008: Simulation of modern and middle Cretaceous marine d18O with an ocean-atmosphere general circulation model. Paleoceanography, 23, PA3223, doi:10.1029/2008PA001596.